hep-ph/9405366

πN Scattering in a Large-N_c σ-Model

Michael P. Mattis* and Richard R. Silbar

Theoretical Division, Los Alamos National Laboratory

Los Alamos, NM 87545 USA

(May 1994)

Abstract

We review the large-N_c approach to meson-baryon scattering, including recent interesting developments. We then study πN scattering in a particular variant of the linear σ-model, in which the couplings of the σ and π mesons to the nucleon are echoed by couplings to the entire tower of $I = J$ baryons (including the Δ) as dictated by large-N_c group theory. We sum the complete set of multi-loop meson-exchange $\pi N \to \pi N$ and $\pi N \to \sigma N$ Feynman diagrams, to leading order in $1/N_c$. The key idea, reviewed in detail, is that large-N_c allows the approximation of *loop* graphs by *tree* graphs, so long as the loops contain at least one baryon leg; trees, in turn, can be summed by solving classical equations of motion. We exhibit the resulting partial-wave S-matrix and the rich nucleon and Δ resonance spectrum of this simple model, comparing not only to experiment but also to πN scattering in the Skyrme model. The moral is that much of the detailed structure of the meson-baryon S-matrix which hitherto has been uncovered only with skyrmion methods, can also be described by models with explicit baryon fields, thanks to the $1/N_c$ expansion.

Typeset using REVTEX

I. OVERVIEW OF THE LARGE-N_C APPROACH TO MESON-BARYON SCATTERING

It is well known [1–6] that QCD simplifies greatly in the limit $N_c \to \infty$, N_c being the number of colors. Not surprisingly, the large-N_c limit has likewise proved to be very useful in studying effective low-energy hadron Lagrangians for the Strong Interactions. Broadly speaking, such effective theories fall into two categories. On the one hand, there is the straightforward Feynman diagrammatic approach in which mesons and baryons are each treated as explicit dynamical fields, while on the other hand, there is the more economical skyrmion picture [7,8] in which baryons are viewed as solitons constructed from the meson degrees of freedom. Since both these approaches purport to describe the low-energy Strong Interactions, it follows that if they are sensible, they should be equivalent to one another. Furthermore, this equivalence must hold order by order in $1/N_c$. The first steps towards establishing such an equivalence are just recently being taken [9–12].

In either approach, a particularly fruitful physical process to examine has been meson-baryon scattering in the large-N_c limit. The present paper furthers this study, taking as a tractable example of a multi-channel Lagrangian a variant of the linear σ-model. Before we specify the model, and our particular treatment of it, it is helpful to put the present work in historical context.

A review of the relevant theoretical literature over the past decade reveals an interesting sociological phenomenon: there are two disjoint bodies of large-N_c papers devoted to two topologically distinct sets of diagrams, namely *Compton-type* versus *exchange-type* graphs, that contribute to the meson-baryon S-matrix.[1] Examples of Compton-type and exchange-type graphs are displayed in Fig. 1 and Fig. 2, respectively. Topologically, they differ in the following way: in the exchange-type graphs of Fig. 2, it is possible to trace a continuous line from the incoming to the outgoing meson without ever traversing a baryon line segment, whereas in the Compton-type graphs of Fig. 1 this cannot be done.

Let us review, briefly, some of the salient points of physics that emerge from the study of each of these two classes of diagrams.

---

[1] So far as we are aware, the only attempt to date to treat these two classes of graphs in a unified manner can be found in Sec. 7 of Ref. [10].

A. Compton-type graphs

While presently the Compton-type graphs (Refs. [11–17]) are much less well understood than the exchange-type graphs discussed below, they nevertheless yield some interesting physics, as follows. Look at Figs. 1a and 1b. Since each vertex scales like $\sqrt{N_c}$ (see Ref. [3]), these graphs individually scale like[2] N_c. However, we know from Witten's analysis of quark-gluon diagrams [3] that the total amplitude for meson-baryon scattering must scale like N_c^0, not N_c. Therefore there must be leading-order cancellations between Figs. 1a and 1b. Add to this observation another important piece of large-N_c physics: the fact that for the case of two light flavors (which we focus on exclusively herein) the spectrum of stable baryons is a tower of states of equal spin and isospin [8]: $I = J = 1/2, 3/2, 5/2, \cdots, N_c/2$, which are all degenerate in the large-N_c limit (more precisely, in the limit $J^2/N_c \to 0$). We then demand leading-order cancellation between Figs. 1a and 1b, for the reason described above, with the three baryon legs drawn from all possible baryon states in the $I = J$ tower, consistent with triangle inequalities for isospin and angular momentum at each vertex. This exercise is carried out in Refs. [13] and [14]. The upshot is a set of proportionality relations between the various coupling constants $g_{\pi NN}$, $g_{\pi N\Delta}$, $g_{\pi\Delta\Delta}$, and so forth up the $I = J$ tower, relating each of these *a priori* independent couplings to a single underlying coupling constant, up to multiplication by Clebsch-Gordan coefficients. We call this set of relations for the pion-baryon couplings the "proportionality rule." Furthermore, Dashen and Manohar have shown that corrections to the proportionality rule do not occur at order $1/N_c$, as naively expected, but rather at order $1/N_c^2$ [15]. This suggests that the proportionality rule should be relatively robust. Calculationally, it implies that, once the order N_c contributions to the amplitude have cancelled, the surviving order N_c^0 pieces arise solely from the $1/N_c$ corrections to the baryon propagator, and not from $1/N_c$ corrections at the vertices, as one might have thought.

Numerically, the proportionality rule for the pion-baryon couplings works well. Not only does the decay width of the Δ work out to within a few GeV of its measured value when $g_{\pi N\Delta}$ is related, using this rule, to the experimental value of $g_{\pi NN}$ [8,10]; but furthermore, with the same input parameters, the widths of the "large-N_c artifacts," *i.e.* the baryons with $I = J \geq 5/2$, are so large that they cannot be considered "particles" at all, and as such, pose no problem for phenomenology [10]. This latter observation removes what

---

[2] The baryon propagator is approximated by $i(v \cdot k + i\epsilon)^{-1}$ in the large-N_c limit, where v is the baryon's 4-velocity, k is the momentum imparted by the incoming meson (assuming the incoming baryon to be on shell), and it is also understood that one throws away the two small components of the Dirac 4-spinor. We focus on the kinematic regime $k \sim N_c^0$ so that the baryon propagators do not affect the N_c counting.

has been, till recently, one of the chief objections to the entire large-N_c program. Another success of large N_c is that the group-theoretic predictions of the old $SU(2N_F)$ symmetry are recaptured [5,6,14,16], without the need to appeal to the construct of the nonrelativistic, weakly interacting constituent quark model.

A further refinement was made recently by Jenkins [17], who examined the one-loop chiral corrections to the masses M_J of the $I = J$ baryons, and deduced the consistency relations

$$M_J \;=\; M_0 \;+\; \frac{J(J+1)}{2\mathcal{I}} \;+\; \mathcal{O}(N_c^{-2}) \tag{1}$$

where M_0 and $\mathcal{I}$ are constants of order N_c that can be fixed, for example, by pegging $M_{1/2}$ and $M_{3/2}$, respectively, to the experimental nucleon and Δ masses.

While the large-N_c results of Refs. [14–17] are derived using effective Lagrangians of mesons and explicit baryons, the physics of the Compton-type graphs can also be accessed using the skyrmion approach [11,12]. The parallelism between the two approaches is manifest in expressions such as Eq. (1). In the language of the two-flavor Skyrme model, M_0 and $\mathcal{I}$ are interpreted as the mass and moment of inertia of the soliton, respectively [8,18]. It is reassuring that the expression (1) can also be gotten directly from looking at quark diagrams in large-N_c QCD [5,6], closing the circle.

B. Exchange-type graphs

Next we turn to the physics of the exchange-type graphs (Refs. [9,19–27]), which is the primary focus of this paper. Examples are shown in Fig. 2. These graphs likewise contribute to the scattering amplitude starting at order N_c^0. Although the summation of *all* such graphs would appear to be an impossible task, it can actually be carried out in a straightforward manner—so long as one contents oneself with the leading-order answer in the $1/N_c$ expansion [9]. As will be reviewed in detail in the Sections to follow, the key idea is to rewrite these multiloop graphs as *trees*, exploiting the large-N_c approximation. Tree graphs have the great advantage over loops that they can all be summed by solving *classical* equations of motion.[3]

[3] To remind the reader [9] that he or she already knows a situation where "loops" become "trees," recall the ancient problem of electron-proton scattering in the low-energy regime where the proton mass is much greater than all other scales in the problem. On the one hand, these are evidently multiloop interactions, in which the proton and electron lines exchange a large number of photons in all possible tanglings. On the other hand, we know that the physics is accurately described by *classical* equations: first the proton generates a classical Coulomb field, and then the electron propagates linearly through this non-trivial background (Rutherford scattering). These two dis-

It is this summability property which justifies our earlier statement that the exchange-type graphs are much better understood than the Compton-type graphs.

While the analysis of this paper will be carried out using explicit baryon fields, the set of classical equations that emerges is, once again, highly reminiscent of the skyrmion approach, in which the corresponding classical equations describe a pion propagating through the background field generated by the skyrmion itself [19–24]. In particular, the group-theoretic relations familiar from the Skyrme model carry over intact to models such as the present one with explicit baryons. These include non-trivial, and experimentally reasonably well satisfied, relations in which isospin-3/2 πN scattering amplitudes are expressed as linear combinations of the isospin-1/2 amplitudes [19,22]. Similar relations hold for kaon-nucleon scattering [23], and for $\pi N \to \rho N$ [24], and in fact for all quasielastic meson-baryon scattering processes.

If, extending Donohue's original suggestion [25], one crosses these relations among scattering amplitudes from the s-channel to the t-channel (*e.g.*, $N\bar{N} \to$ mesons), they can be re-expressed concisely as two large-N_c selection rules [26,27]. First, there is the very same "proportionality rule" discussed earlier, in the context of the Compton-type graphs. However, the derivation given in Ref. [26] makes clear that the proportionality rule is *completely independent of the chiral limit*, and furthermore, that it applies not only to the pion-baryon couplings but equally to the baryon couplings of *all* bosons. Beyond the width calculations noted above [8,10], the phenomenological validity of the proportionality rule is put to the test in Fig. 7 of Ref. [22], in which the appropriate linear combinations of the experimental $\pi N \to \pi N$ and $\pi N \to \pi\Delta$ scattering amplitudes are compared.

In addition, a second large-N_c selection rule emerges, the "$I_t = J_t$ rule" [26,27]. This rule states that the isospin of the emitted/absorbed meson must equal its *total* (spin + orbital) angular momentum, measured in the rest frame of the large-N_c baryon. Concrete examples of meson-nucleon couplings that satisfy the $I_t = J_t$ rule include the pseudovector coupling of the pion, the tensor coupling of the ρ, and the vector coupling of the ω [27]:

$$(g_{\pi NN}/2M_N)\partial_\mu\vec{\pi}\cdot\bar{N}\gamma^5\gamma^\mu\vec{\tau}N \ , \quad g_\rho^{\rm tens}\partial_\mu\vec{\rho}_\nu\cdot\bar{N}\sigma^{\mu\nu}\vec{\tau}N \ , \quad g_\omega^{\rm vec}\omega_\mu\cdot\bar{N}\gamma^\mu N \ , \tag{2}$$

each of which must be augmented by couplings to the entire tower of $I = J$ baryons as required by the proportionality rule. Since these couplings obey the $I_t = J_t$ rule, the three coupling constants are nonvanishing at leading order in the large-N_c expansion:

---

parate pictures are reconciled by the fact that the loop graphs are really trees, by exactly the same manipulations described in Sec. II below. The insight of Ref. [9] is that this same mechanism (modulo nonlinearities due to the fact that bosons, unlike photons, are self-interacting) holds for the exchange of arbitrary bosons in the large-N_c limit, thanks to the proportionality rule as well as the $I_t = J_t$ rule reviewed below.

$$\frac{g_{\pi NN}}{2M_N} \sim g_\rho^{\rm tens} \sim g_\omega^{\rm vec} \sim \sqrt{N_c}\ . \tag{3}$$

In contrast, the $I_t = J_t$ rule *forbids* at leading order the other two canonical vector-meson interactions, the *vector* coupling of the ρ and the *tensor* coupling of the ω,

$$g_\rho^{\rm vec}\vec{\rho}_\mu \cdot \bar{N}\gamma^\mu\vec{\tau}N \quad \text{and} \quad g_\omega^{\rm tens}\partial_\mu\omega_\nu \cdot \bar{N}\sigma^{\mu\nu}N\ , \tag{4}$$

meaning that these coupling constants must be down by (at least) one power of $1/N_c$ compared to Eq. (3):

$$g_\rho^{\rm vec} \sim g_\omega^{\rm tens} \sim \frac{1}{\sqrt{N_c}}\ . \tag{5}$$

The relative unimportance of the vector (tensor) coupling of the ρ (ω) has long been known to nuclear physicists who construct one-boson exchange models of the nucleon-nucleon potential [28–31]. It is pleasing to see these phenomenological rules of thumb emerge as theorems in the large-N_c limit.

C. Two interesting unresolved questions

In lieu of a Conclusions section, we close this expanded Introduction with two questions that are food for further thought. First, is the complete meson-baryon S-matrix properly obtained by adding the Compton-type and exchange-type graphs together, or, as an alternative prescription, might it be the case that either set of graphs *by itself* (assuming an infinite spectrum of mesons) contains the complete answer? This latter possibility is suggested by the observation that mesons and baryons are composite particles made up from quarks and gluons. Since at the quark-gluon level there is no longer a topological distinction between the graphs of Fig. 1 and Fig. 2, one must be especially careful to avoid double counting, and this might conceivably preclude adding the graphs of Fig. 1 and Fig. 2 together in a naive way.[4]

Second, the exchange-graph formalism of Ref. [9] applies not only to the meson-baryon system which we focus on here, but equally to the baryon-baryon, baryon-antibaryon, baryon-baryon-baryon, and in general to all n-baryon, m-antibaryon interactions (Fig. 3). Of course, there are no analogs of Compton-type graphs for these multi-baryon systems. It follows that the exchange-graph formalism of Ref. [9] gives—in principle—*the complete*

[4] For the resolution of similar issues in atomic physics, namely the avoidance of double-counting when bound states are involved, see Ref. [33] and references therein.

answer for these cases, to leading order in $1/N_c$. By this we specifically mean the following: given an effective hadron Lagrangian whose meson-baryon couplings properly embody the $I_t = J_t$ and proportionality rules, the complete set of Feynman diagrams of the sort exhibited in Fig. 3 can be summed to leading order in $1/N_c$. It would be an interesting exercise to carry out this program, starting from a well-motivated effective Lagrangian, and to compare the results to the popular Bonn [30] and Paris [31] potential models (which are derived from just the ladder diagrams with at most one crossing) as well as to the recent work of Weinberg and others that relies exclusively on chiral perturbation theory [34].

D. Outline of paper

The remainder of this paper is organized as follows. In Sections II and III we review the exchange-graph formalism of Ref. [9] and apply it to two warm-up problems, a "σ-only" and a "π-only" model, respectively. Sections IV-VI explore in detail the meson-baryon S-matrix in a richer model comprising both pions and σ mesons, a variation on the Gell-Mann-Levy σ-model [32]. Obviously, we do not take this model seriously as a realistic depiction of hadron physics. Rather, we aim only to illustrate how the formalism of Ref. [9] leads in a concrete way to a quantitative calculation of the exchange-graph contribution to the multi-channel meson-baryon S-matrix. With the present model solved, the scene is set for more ambitious, realistic calculations, necessarily incorporating vector mesons. We are also interested in comparing the large-N_c effective Lagrangian approach that uses explicit baryons, with earlier large-N_c results from the Skyrme model. We come to the conclusion that much of the detailed structure of the meson-baryon S-matrix which hitherto has been uncovered only with skyrmion methods, can equally be described by models with explicit baryon fields. At the same time, both approaches share significant problems in the low partial waves, the complete resolution of which remains a major technical hurdle.

II. FIRST WARM-UP PROBLEM: A σ-ONLY MODEL

As a first calculation, let us consider a model with only σ mesons and (non-strange) baryons [9,35]. Because the σ has $I = J = 0$, this toy model avoids the spin and isospin complications due to non-commutativity of Pauli matrices at the meson-nucleon vertices. It also avoids the complications of inelastic 2-body channels (*e.g.*, nucleons cannot turn into Δ's).

The Lagrangian to be solved in this Section is the large-N_c version of:

$$\mathcal{L}_{\sigma N} = \frac{1}{2}(\partial_\mu \sigma)^2 - V(\sigma) + \overline{N}(i\gamma\cdot\partial - M_N)N - g\sigma\overline{N}N \ , \tag{6}$$

where, for definiteness, the σ self-interactions are described by the fourth-order potential

$$V(\sigma) = \frac{1}{2}{m_\sigma}^2\sigma^2 + \frac{1}{6}\kappa\sigma^3 + \frac{1}{24}\lambda\sigma^4 \ . \tag{7}$$

By the words "large-N_c version of" we mean that the coupling of the σ to the nucleon in Eq. (6) must, in principle, be augmented by analogous couplings to the entire $I = J$ tower of large-N_c baryons, starting with the Δ ($I = J = 3/2$) and continuing through the state with $I = J = N_c/2$. The relative strengths of these couplings is given by the proportionality rule [26]. However, in this simple model, since the σ carries the quantum numbers of the vacuum, it couples diagonally to this tower (as noted above). Therefore, so long as we restrict our attention to nucleon targets, we can safely drop these additional couplings to the higher baryon states and work with the simplified Lagrangian (6).

In the large-N_c limit the nucleon has mass of order N_c and its degrees of freedom freeze out. This means that the nucleon kinetic energy term in Eq. (6) can be dropped, and the Yukawa term has $\overline{N}N$ replaced by a static source $j(\mathbf{x})$. The formal derivation of this intuitive prescription was given in Ref. [9]. For completeness, we review it here. Looking at Fig. 4, the product of the nucleon propagators (reading from bottom to top) is

$$\begin{aligned}\frac{i}{\not p + \not k_1 - M_N + i\epsilon}\times\frac{i}{\not p + \not k_1 + \not k_2 - M_N + i\epsilon}\times\cdots\times\frac{i}{\not p + \not k_1 + \cdots + \not k_{n-1} - M_N + i\epsilon} \\ \approx \ \frac{\gamma_0+1}{2}\frac{i}{k_{10}+i\epsilon}\times\cdots\times\frac{i}{k_{10}+\cdots+k_{n-1,0}+i\epsilon} \ .\end{aligned} \tag{8}$$

In the above we have taken the large-N_c (*i.e.*, nonrelativistic) limit of the nucleon propagators

$$\frac{i}{\not p + \not k - M_N + i\epsilon} \quad \stackrel{N_c\to\infty}{\longrightarrow} \quad \frac{\gamma_0+1}{2}\frac{i}{k_0+i\epsilon} \ , \tag{9}$$

assuming that the nucleon is in its rest frame. The prefactor $(\gamma_0 + 1)/2$ is the projector onto the large components of the Dirac 4-spinor. From now on we suppress it, with the understanding that we always throw away the small components.

Our desired result is obtained by summing over the $n!$ crossed ladders (Fig. 5), and using the interesting identity for distributions,

$$\begin{aligned}2\pi\delta(\sum_{i=1}^n k_{i0}) \sum_{\substack{\text{permutations}\\(i_1,\cdots,i_n)}} \frac{i}{k_{i_1 0}+i\epsilon}\times\frac{i}{k_{i_1 0}+k_{i_2 0}+i\epsilon}\times\cdots\times\frac{i}{k_{i_1 0}+\cdots+k_{i_{n-1}0}+i\epsilon} \\ = 2\pi\delta(k_{10})\times 2\pi\delta(k_{20})\times\cdots\times 2\pi\delta(k_{n0}) \ .\end{aligned} \tag{10}$$

(To prove this, Fourier transform both sides of this identity in all n momenta.) Each of the $n!$ terms in this sum corresponds to a distinct crossing or ordering of the n rungs of the

ladder. The δ-function on the left-hand side of this equation reflects conservation of energy along the nucleon line in the large-N_c limit:

$$2\pi\delta(\,-p_0'+p_0+\sum_{i=1}^{n}k_{i0}) \quad \stackrel{N_c\to\infty}{\longrightarrow} \quad 2\pi\delta(\,\sum_{i=1}^{n}k_{i0})\ . \tag{11}$$

Recognizing $2\pi\delta(k_0)$ as the 4-dimensional Fourier transform of $\delta^3(\mathbf{x})$, we immediately understand the meaning of the simple factorized right-hand side of Eq. (10) in terms of graphs. Simply put, the sum of the $n!$ crossed ladders is equal to the *single* graph of Fig. 6, generated by the effective Lagrangian

$$\mathcal{L}_{\rm eff} \ = \ \frac{1}{2}(\partial_\mu\sigma)^2 - V(\sigma) - \sigma j(\mathbf{x}) \tag{12}$$

where, as promised, the nucleon field has been frozen out in favor of the external c-number source

$$j(\mathbf{x}) \ = \ g\,\delta^3(\mathbf{x})\ . \tag{13}$$

The complete exchange-graph contribution to σN scattering in the large-N_c limit now emerges from a two-stage numerical program, which is most transparent in graphical terms. In the first stage, one defines a "classical" σ field $\sigma_{\rm cl}$ as the sum of all one-point trees (Fig. 7). The reason one considers only trees is that meson loops are suppressed by powers of $1/N_c$ [2,3,6]. In the second stage, one considers a propagating σ field (which we call the "quantum" field $\sigma_{\rm qu}$ to distinguish it from $\sigma_{\rm cl}$) interacting with an arbitrary number of $\sigma_{\rm cl}$ insertions (Fig. 8). By inspection, this two-stage procedure is equivalent to summing all the tree graphs of the form shown in Fig. 6 (the loop graphs being subleading in $1/N_c$). As promised: the loops (Figs. 4-5) have turned into trees, exactly as in the old electron-proton problem invoked in Sec. I.

This two-stage graphical procedure is easily translated into the language of differential equations. Solving for $\sigma_{\rm cl}$ as per Fig. 7 is equivalent to solving the classical Euler-Lagrange equation for the effective Lagrangian of Eq. (12), namely,

$$-\,\nabla^2\sigma_{\rm cl}(\mathbf{x}) + V'(\sigma_{\rm cl}(\mathbf{x})) + j(\mathbf{x}) \ = \ 0\ . \tag{14}$$

Note that $\sigma_{\rm cl}$ is time-independent because the source $j(\mathbf{x})$ has this property. Next, solving for the propagating field $\sigma_{\rm qu}$, as given by Fig. 8, is accomplished by noticing that at every vertex, there are exactly two $\sigma_{\rm qu}$ legs, the rest being insertions of $\sigma_{\rm cl}$, with the coupling constants read off from $V(\sigma)$. Therefore, the relevant equation of motion comes from the *quadraticized* Lagrangian

$$\mathcal{L}_{\rm quad} \ = \ \frac{1}{2}\partial_\mu\sigma_{\rm qu}\partial^\mu\sigma_{\rm qu} - \frac{1}{2}\sigma_{\rm qu}^2 V''(\sigma_{\rm cl}(\mathbf{x}))\ , \tag{15}$$

which induces the linear time-dependent equation

$$[\partial_\mu \partial^\mu + V''(\sigma_{\rm cl}(\mathbf{x}))]\ \sigma_{\rm qu}(x) \ = \ 0 \ . \tag{16}$$

In short, we have outlined a two-stage numerical procedure, the first stage involving a non-linear time-independent equation for a "classical" meson field, the second involving a linear time-dependent equation for a "quantum" meson field in the classical background. This is reminiscent of the skyrmion approach to meson-baryon scattering [19–22]. In the subsequent Sections, when pions are introduced, this correspondence will be sharpened by the emergence of a hedgehog structure to the classical pion field that is familiar from the Skyrme model [7,8]. (The chief *difference* between the two approaches is, of course, that baryon number is carried by topology in the Skyrme model, and by smeared δ-function sources when the baryon fields are explicit.)

The analog of the hedgehog Ansatz in the present model with $I = 0$ σ mesons alone is just ordinary spherical symmetry:

$$\sigma_{\rm cl}(\mathbf{x}) \equiv G(r) \ . \tag{17}$$

The profile function $G(r)$ is found by solving the non-linear radial differential equation

$$G'' + \frac{2}{r} G' - {m_\sigma}^2 G - \frac{\kappa}{2}\, G^2 - \frac{\lambda}{6}\, G^3 = j(\mathbf{x}) \tag{18}$$

implied by Eqs. (7) and (14). Unfortunately, Eq. (18) suffers from ultraviolet problems when j is literally taken to be a δ-function as per Eq. (13). The source of these divergences (which are worse than in the original loop graphs, Figs. 4-5) can be traced to the nonrelativistic reduction of the propagator (9), which is only valid so long as the components of the exchanged meson momentum satisfy $|k_\mu| \ll M_N$. (A similar breakdown of the large-N_c approach is discussed in Sec. 8 of Ref. [3].) A simple cure is to smear out the source, say, as a Gaussian:

$$j(\mathbf{x}) \ \longrightarrow \ \frac{g}{(a_N \sqrt{\pi})^3} \exp(-r^2/a_N^2) \ , \quad a_N \sim N_c^0 \ . \tag{19}$$

This approximation now renders Eq. (18) tractable, at the expense of introducing a "nucleon size" parameter a_N into the problem. This new parameter provides an ultraviolet cutoff on the momentum allowed to flow into or out of the nucleon. We have checked that our numerical results are not overly sensitive to a_N over a reasonable range of values.

Equation (18) represents a two-boundary value problem which can be solved in an iterative fashion using a standard "shoot and match" Runge-Kutta integration procedure [36].[5]

---

[5] For details, see the Appendix.

Fig. 9 shows the profile function $G(r)$ for the specific choice of parameters $m_\sigma = 600\,\mathrm{MeV}$, $\kappa = 18.5$, $\lambda = 214$, $g = 13.6$ and $a_N = 0.5$ fm. Note that $G(r)$ looks very much like a Yukawa function, $\exp(-m_\sigma r)/r$, except that it is finite at the origin (because of the smearing of the nucleon source term) and has small deviations in the 0.5 to 1.0 fm region due to the non-linear terms involving κ and λ.

Given $G(r)$, we then solve Eq. (16) for $\sigma_{\rm qu}$ by means of a standard partial wave analysis. For angular momentum l, the radial scattering wave function $u_l(r) = r\sigma_l(r)$ having energy ω satisfies

$$\left[\frac{d^2}{dr^2} + q^2 - \kappa G(r) - \frac{\lambda}{2}G^2(r) - \frac{l(l+1)}{r^2}\right] u_l(r) = 0\ , \quad q^2 = \omega^2 - m_\sigma^2\ . \tag{20}$$

This is a Schrödinger-like linear differential equation that can also be solved by Runge-Kutta integration from the origin (where $u_l(r)$ must be regular, going like r^{l+1}). The asymptotic form of $u_l(r)$ is then fit in the usual way to a linear combination of spherical Ricatti-Bessel functions, $j_l(qr)$ and $n_l(qr)$, yielding the phase shifts for σN elastic scattering.

The potential in Eq. (16) [or Eq. (20)] has a short-range repulsive core (coming from the quartic term in the Lagrangian) and intermediate-range attraction (coming from the cubic term and the fact $G(r) < 0$). Consequently, as shown in Fig. 10, the S-wave phase shift at low energies is positive because of the medium-range attraction, but it soon turns over and looks like the phase shift for a hard-core repulsive potential. At still higher energies (not shown), the phase shift returns to 0, since the short-range repulsive core is finite. The higher partial waves exhibit similar behavior, but offset to increasingly higher energies because of the angular momentum barrier.

III. SECOND WARM-UP PROBLEM: A π-ONLY MODEL

As a second simplified example, we consider a model of gradient-coupled pions and $I = J$ baryons. The Lagrangian we want to solve is the large-N_c version of

$$\begin{aligned}\mathcal{L}_{\pi N} = {} & \frac{1}{2}\partial_\mu\pi^a\,\partial^\mu\pi^a - \frac{1}{2}m_\pi^2\,\pi^a\pi^a - \frac{\lambda}{24}(\pi^a\pi^a)^2 \\ & + \overline{N}(i\gamma\cdot\partial - M_N)N - g_\pi\partial_\mu\vec{\pi}\cdot\overline{N}\gamma^5\gamma^\mu\vec{\tau}N\ .\end{aligned} \tag{21}$$

The reason for choosing pseudovector coupling rather than the pseudoscalar coupling, $-g'_\pi\vec{\pi}\cdot\overline{N}i\gamma^5\vec{\tau}N$, is that it is more amenable to a large-N_c treatment, for the following reason. The matrix γ^5 is purely off-diagonal, connecting the large to the small components of the Dirac 4-spinor. This means that taking the nonrelativistic limit of the baryons is a singular operation when the pion is not soft. In contrast, $\gamma^5\gamma^\mu$ does connect the large components

to themselves for $\mu = 1, 2, 3$ so that, with a pseudovector coupling, we can follow the simple leading-order large-N_c prescription given earlier of just throwing away the small components (including, *inter alia*, the $\gamma^5\gamma^0$ contribution; remember that the $1/N_c$ expansion breaks up Lorentz invariants). Of course, in a different limit from large N_c, namely the soft-pion limit in which the pion is emitted from the on-shell nucleon at approximately zero 4-momentum, the pseudovector and pseudoscalar couplings are indistinguishable, provided one takes $g_\pi = g'_\pi/2M_N$.

The meaning of the words "large-N_c version of" preceding the Lagrangian (21) is that, as in the σN model of the previous section, the coupling of the pion to the nucleon must be supplemented by analogous couplings to all the other members of the tower of $I = J$ baryons, and likewise for the nucleon kinetic term. In the previous case this was an irrelevant complication: because the zero-isospin σ cannot induce transitions between states in this tower, the problem diagonalizes. In contrast, pions can and do change nucleons to Δ's, etc.

The most convenient way to implement the gradient coupling of the pion to the $I = J$ tower of baryons is to change baryon basis to the so-called collective coordinate basis $|A\rangle$ familiar from the Skyrme model, with A an $SU(2)$ element [8]. These basis elements are defined by [8,18].

$$|A\rangle \;=\; \sum_{R=1/2,\,3/2,\cdots} (2R+1)^{1/2} \sum_{i_z,s_z=-R,\cdots,R} (-)^{R-s_z} D^{(R)}_{-s_z,i_z}(A^\dagger) \left| \begin{matrix} R \\ i_z\; s_z \end{matrix} \right\rangle \;, \tag{22}$$

normalizing the volume of $SU(2)$ to unity. On the right-hand side of this equation, the baryons are given in the usual spin-isospin basis, e.g., a neutron of spin up and a Δ^+ of spin projection $-3/2$ would be denoted as $\left| \begin{smallmatrix} 1/2 \\ -1/2,1/2 \end{smallmatrix} \right\rangle$ and $\left| \begin{smallmatrix} 3/2 \\ 1/2,-3/2 \end{smallmatrix} \right\rangle$, respectively. In the collective coordinate language, the correct pion-baryon coupling reads

$$-\,3g_\pi \sum_{a,b=-1,0,1} \partial_b \pi^a \int_{SU(2)} dA\, D^{(1)}_{ab}(A)\, |A\rangle\, \langle A| \;\; . \tag{23}$$

This coupling was first written down on general grounds (without reference to soliton physics) by Adkins, Nappi and Witten [8], and is necessary for the consistency of the Compton-type graphs with the overall N_c^0 scaling of the pion-baryon scattering amplitude in the large-N_c limit, as reviewed earlier [13,14]. It has also recently been established using collective coordinate quantization of the skyrmion [10]. Despite our convenient adoption of Skyrme-model notation, we emphasize that the coupling (23) is, in the present context, understood to be built from explicit baryon field operators, and not solitons.

Let us verify explicitly that Eq. (23) is indeed the correct large-N_c pseudovector coupling of the pion to the baryon tower. In particular, Eq. (23) has the following four desirable properties:

1. It is invariant under isospin and angular momentum;

2. It contains the pion-nucleon interaction shown in Eq. (21);

3. It correctly implements the "proportionality rule" governing couplings to the higher states in the $I = J$ tower.

4. It accurately predicts the width of the Δ, and furthermore, gives widths so large for the large-N_c artifacts of the model (the baryons with $I = J \geq \frac{5}{2}$) that these pose no phenomenological problems for the large-N_c approach.

We deal with each of these assertions in turn:

1. The state $|A\rangle$ transforms as

$$|A\rangle \stackrel{\text{isospin}}{\longrightarrow} |U_I A\rangle \quad \text{and} \quad |A\rangle \stackrel{\text{ang.mom.}}{\longrightarrow} \left|AU_J^\dagger\right\rangle \tag{24}$$

so that

$$\begin{aligned}\int_{SU(2)} dA\, D^{(1)}_{ab}(A)|A\rangle\langle A| \;&\longrightarrow\; \textstyle\int_{SU(2)} dA\, D^{(1)}_{ab}(A) \left|U_I A U_J^\dagger\right\rangle \left\langle U_I A U_J^\dagger\right| \\ &= \textstyle\int_{SU(2)} dA\, D^{(1)}_{ab}(U_I^\dagger A U_J)\, |A\rangle\, \langle A| \\ &= D^{(1)}_{aa'}(U_I^\dagger) D^{(1)}_{bb'}(U_J^\dagger) \textstyle\int_{SU(2)} dA\, D^{(1)}_{a'b'}(A)\, |A\rangle\, \langle A| \;. \end{aligned} \tag{25}$$

Here we have used the group invariance of the $SU(2)$ measure, $d(U_I^\dagger A U_J) = dA$, and the reality property of the $D^{(1)}$ matrices. Similarly,

$$\partial_b \pi^a \;\longrightarrow\; \partial_{b''} \pi^{a''} D^{(1)}_{a''a}(U_I) D^{(1)}_{b''b}(U_J) \;. \tag{26}$$

Combining these last two equations and using the composition property of the Wigner D matrices, we confirm that the coupling of Eq. (23) *is* invariant under isospin and angular momentum rotations.

2. Using Eq. (22), we rewrite the coupling of Eq. (23) as

$$\begin{aligned} -3g_\pi \sum_{a,b} \partial_b \pi^a \quad & \sum_{R, i_z, s_z} \sum_{R', i'_z, s'_z} (-)^{R - s_z} (-)^{R' - s'_z} [(2R+1)(2R'+1)]^{1/2} \left| \begin{matrix} R' \\ i'_z\; s'_z \end{matrix} \right\rangle \left\langle \begin{matrix} R \\ i_z s_z \end{matrix} \right| \\ & \qquad \times \int_{SU(2)} dA\, D^{(1)}_{ba}(A^\dagger) D^{(R')*}_{-s'_z, i'_z}(A^\dagger) D^{(R)}_{-s_z, i_z}(A^\dagger) \\ = \; -3g_\pi \sum_{a,b} \partial_b \pi^a & \sum_{R, i_z, s_z} \sum_{R', i'_z, s'_z} (-)^{R+R'} \langle R\, 1\, i_z\, a | R'\, i'_z \rangle \langle R'\, 1\, s'_z\, b | R\, s_z \rangle \\ & \qquad \times \left| \begin{matrix} R' \\ i'_z\; s'_z \end{matrix} \right\rangle \left\langle \begin{matrix} R \\ i_z s_z \end{matrix} \right| \;, \end{aligned} \tag{27}$$

using standard D-matrix integration tricks. We now pick out the terms with $R = R' = 1/2$ in this expression in order to study specifically the pion coupling to $\overline{N}N$. Isospin and angular momentum invariance can be made more manifest by rewriting this subset of terms as

$$g_\pi \sum_{a,b} \sum_{i_z,s_z} \sum_{i'_z,s'_z} \tau^a_{i'_z\, i_z} \sigma^b_{s'_z\, s_z}\, \partial_b \pi^a \left| \begin{matrix} 1/2 \\ i'_z\, s'_z \end{matrix} \right\rangle \left\langle \begin{matrix} 1/2 \\ i_z s_z \end{matrix} \right| \tag{28}$$

which we recognize as the nonrelativistic (or, equivalently, in the present context, large-N_c) limit of the gradient coupling $-g_\pi \partial_\mu \vec{\pi} \cdot \overline{N} \gamma^5 \gamma^\mu \vec{\tau} N$.

3. A careful reading of Ref. [26] reveals this criterion will be automatically satisfied due to the diagonality of the pion-baryon coupling, Eq. (23), in the collective coordinate A. It is instructive nevertheless to see how this comes about explicitly. The baryon-antibaryon Hilbert-space operator in Eq. (27) can be written in terms of states with good t-channel (exchange-channel) quantum numbers as follows:

$$\begin{aligned} \left| \begin{matrix} R' \\ i'_z\, s'_z \end{matrix} \right\rangle \left\langle \begin{matrix} R \\ i_z s_z \end{matrix} \right| \;=\; & \sum_{I_t,I_{tz}} \sum_{J_t,J_{tz}} (-)^{R+i_z} (-)^{R'+s'_z} \langle I_t I_{tz} | R' R i'_z, -i_z \rangle \langle R R' s_z, -s'_z | J_t J_{tz} \rangle \\ & \times \left| \begin{matrix} I_t\,;\, RR' \\ I_{tz} \end{matrix} \right\rangle \left\langle \begin{matrix} J_t\,;\, RR' \\ J_{tz} \end{matrix} \right| , \end{aligned} \tag{29}$$

where the phases in the above are the usual cost of turning bras into kets in $SU(2)$ [37]: $|jm\rangle \leftrightarrow (-)^{j+m} \langle j, -m|$. Plugging Eq. (29) into Eq. (27) and using Clebsch-Gordan orthogonality gives for the pion-baryon coupling:

$$-\, g_\pi \sum_{I_{tz},J_{tz}} \partial_{J_{tz}} \pi^{I_{tz}} \sum_{R,R'} (-)^{R+R'} [(2R+1)(2R'+1)]^{1/2} \left| \begin{matrix} I_t = 1\,;\, RR' \\ I_{tz} \end{matrix} \right\rangle \left\langle \begin{matrix} J_t = 1\,;\, RR' \\ J_{tz} \end{matrix} \right| \tag{30}$$

This equation correctly embodies two large-N_c selection rules: the fact that the exchanged angular momentum J_t is equated to the isospin $I_t = 1$ of the pion is a specific example of the more general $I_t = J_t$ rule [26,27], whereas the square-root proportionality factors relating the pion's couplings to the various baryon states in the $I = J$ tower illustrate the proportionality rule [26].

4. The coupling (23) can be used to calculate the decay width of a baryon with spin/isospin J to the next-lower state $J - 1$ via the emission of a single pion. For the case $\Delta \to N\pi$ one calculates $\Gamma_\Delta = 114\,\mathrm{GeV}$ as against a measured width of 120±5 MeV [8,10]. Pleasingly, for the higher states, $I = J \geq \frac{5}{2}$, the widths turn out to be so large that these large-N_c artifacts cannot be said to exist as particles, and therefore, pose no phenomenological problem for the large-N_c program. One finds $\Gamma_{\frac{5}{2}} \approx 800\,\mathrm{MeV}$, $\Gamma_{\frac{7}{2}} \approx 2600\,\mathrm{MeV}$, $\Gamma_{\frac{9}{2}} \approx 6400\,\mathrm{MeV}$, and so forth [10].

As before, we seek to sum the set of exchange-type graphs of the form shown in Fig. 2. However, *a priori*, the situation is not so simple as in the σ-only model of Sec. II. Look again at the interesting identity (10) for distributions, which is the key to turning loops into trees. The $n!$ terms on the left-hand side correspond to the $n!$ distinct "tanglings" in which the exchanged σ lines are attached in a different order to the baryon line. Because the σ

carries no spin or isospin, each tangling enters with the same relative group-theoretic weight in Eq. (10), and the identity goes through as written (so, too, for photon exchange). In contrast, π, ρ and ω mesons, etc., carry non-trivial isospin and/or spin, and the $n!$ tanglings would not be expected to occur with the same group-theoretic factors. (Pauli spin/isospin matrices do not commute.) Specifically, one expects a different product of n spin and n isospin Clebsch-Gordan factors weighting each term on the left-hand side of Eq. (10), and destroying the identity. Nevertheless, acting together, the $I_t = J_t$ and proportionality rules assure that, to *leading* order in $1/N_c$, these $n!$ group-theoretic factors are indeed equal, once the intermediate baryon legs are summed over all allowed $I = J$ states. Therefore, the identity (10), derived for σ (or photon) exchange, applies as well to the exchange of these non-trivial mesons. This theorem is proved in Ref. [9], using elementary properties of $6j$ symbols. However, there is an easier way to see this, which is to work directly in the $|A\rangle$ basis. So, look again at Fig. 5, and understand the baryon line to mean, not a nucleon or a Δ or any specific member of the $I = J$ tower (which can change identity at each pion interaction vertex), but rather a baryon state $|A\rangle$ sharp in the $SU(2)$ collective coordinate A, which is *preserved* at each vertex, due to the diagonality in A of the coupling (23). Initial and final nucleon, Δ, etc., states can be projected out at the very end of the calculation using standard group-theoretic techniques borrowed from the Skyrme model [i.e., inverting Eq. (22)]. At earlier stages, however, we can use the full machinery of Sec. II to turn loops into trees with impunity.

Therefore, once again, the graphs of Fig. 5 can be summed following a two-stage program. In the first stage, one solves a static non-linear equation for $\vec{\pi}_{\rm cl}(A)$ (noting that the classical pion field depends on the $SU(2)$ collective coordinate A). Isospin covariance trivially relates this quantity to $\vec{\pi}_{\rm cl}(A = 1)$, henceforth called just $\vec{\pi}_{\rm cl}$. Using $D^{(1)}_{ab}(A = 1) = \delta_{ab}$, one obtains the Euler-Lagrange equation

$$-\nabla^2\pi^a_{\rm cl} + m_\pi^2\pi^a_{\rm cl} + \frac{1}{6}\lambda\pi^a_{\rm cl}\vec{\pi}_{\rm cl}\cdot\vec{\pi}_{\rm cl} - 3g_\pi\partial_a\delta^3(\mathbf{x}) \;=\; 0\;. \tag{31}$$

This equation is solved by smearing the δ-function source to a Gaussian as in Eq. (19), and by assuming a hedgehog Ansatz for the classical pion field (anticipating the resemblance to the Skyrme model):

$$\pi^a_{\rm cl}(\mathbf{x}) = \hat{\mathbf{r}}^a F(r)\;. \tag{32}$$

Equation (31) then becomes an ODE for the classical pion profile $F(r)$:

$$F'' + \frac{2}{r}F' \;-\; (\frac{2}{r^2} + m_\pi^2)\;F - \frac{\lambda}{6}F^3 = \;-\frac{6g_\pi r}{a_N^5\pi^{3/2}}\;\exp(-r^2/a_N^2)\;, \tag{33}$$

subject to the boundary conditions that $F(r)$ be regular near $r = 0$ and bounded as $r \to \infty$,

$$F(r) = Br + \mathcal{O}(r^3) \text{ near } r = 0;$$
$$F(r) \to C\exp(-m_\pi r)/r \text{ as } r \to \infty \ . \tag{34}$$

B and C are scale parameters that are initially unknown to us but are fixed implicitly by the non-linearity of Eq. (33). This is another two-boundary-value problem, which can be numerically solved as before (see Fig. 11, and Appendix A).

In the second stage, one solves the linearized time-dependent equation for $\pi_{\rm qu}$ propagating in the background of $\pi_{\rm cl}(A)$. Again, isospin invariance trivially relates this process to the propagation of $\pi_{\rm qu}$ in the background of $\pi_{\rm cl}(A = 1)$, the latter quantity being given by Eqs. (32) and (33). Initial and final nucleons or Δ's are then projected from the hedgehog by inverting Eq. (22), using the orthogonality over $SU(2)$ of Wigner D-matrices. Finally, the initial and final pion-baryon systems are combined into states of good total isospin and angular momentum in the usual fashion to give the partial-wave S-matrix for $\pi N \to \pi N$, $\pi N \to \pi\Delta$, etc.

Fortunately, this cumbersome (if straightforward) sequence of group-theoretic steps can be circumvented, once one realizes that they are *identical* to the procedure followed in the Skyrme model [19–22]. Rather than "reinventing the wheel" one can therefore carry over intact the machinery of Refs. [19–22] of K-spin decomposition and $6j$ symbols. We postpone the explicit review of this formalism to Sec. VI, in which we complete the analysis of the richer model containing both pions and σ mesons.

Unfortunately, the pion-only model discussed in this Section is inherently uninteresting phenomenologically. Because of G-parity, the pion-pion interactions can only come from even powers of $\vec{\pi}(x)$, which means that the potentials entering into the coupled Schrödinger-like scattering equations are strictly repulsive. [They are proportional to $\lambda F^2(r)$.] As a result, all πN phase shifts exhibit repulsive behavior (i.e., clockwise motion in the Argand plots with increasing energy). Thus there is no possibility for πN resonances in such a model. We need *something* like the σ meson to provide a range of attraction between π's and N's.

IV. DEFINING THE σ-π MODEL

In view of the two models discussed in the two previous Sections, one might have some hope that a model combining σ and π mesons would provide a more promising (if still crude) description of pion-nucleon interactions. In this model the σ meson will be taken as an "elementary" field, along with the three π fields. Indeed, in the large-N_c limit, the σ, if such a state exists, is necessarily a stable particle, as the decay amplitude to two pions is suppressed by $1/\sqrt{N_c}$.

For guidance in constructing our large-N_c model of pions and σ mesons, and selecting reasonable values of the coupling constants, we recall the linear σ-model of Gell-Mann and Levy: [32]

$$\begin{aligned}\mathcal{L} = \frac{1}{2}\partial_\mu\sigma'\partial^\mu\sigma' + \frac{1}{2}\partial_\mu\vec{\pi}\cdot\partial^\mu\vec{\pi} - \frac{\lambda}{4}(\sigma'^2 + \vec{\pi}\cdot\vec{\pi} - a^2)^2 + \alpha\sigma' \\ -g\sigma'\overline{N}N - g\vec{\pi}\cdot\overline{N}i\gamma^5\vec{\tau}N + \overline{N}i\gamma\cdot\partial N \ .\end{aligned} \tag{35}$$

In this well-known model, the nucleon and σ get their masses through dynamical symmetry breaking, the σ vacuum expectation value v being $g^{-1}M_N$, and chiral symmetry emerges in the limit $\alpha \to 0$. It is convenient to redefine the σ field by subtracting the VEV,

$$\sigma'(x) \ = \ v + \sigma(x) \ . \tag{36}$$

By substituting for σ' and expanding, the four coupling constants $\{g, \lambda, a, \alpha\}$ can be traded for the more physical set of parameters, $\{g, M_N, m_\pi, m_\sigma\}$, using

$$\lambda = \frac{g^2}{2M_N^2}(m_\sigma^2 - m_\pi^2) \ , \qquad \alpha = \frac{{m_\pi}^2 M_N}{g} \ , \qquad a^2 = \frac{M_N^2}{g^2}\frac{(m_\sigma^2 - 3m_\pi^2)}{(m_\sigma^2 - m_\pi^2)} \tag{37}$$

In this paper we will take

$$g = 13.6 \ , \quad M_N = 5.0 \text{ fm}^{-1} \ , \quad m_\pi = 0.7 \text{ fm}^{-1} \ , \quad \text{and} \quad m_\sigma = 5.0 \text{ fm}^{-1} \ . \tag{38}$$

This choice for the nucleon mass roughly averages the actual N and Δ masses, while the σ meson here could be identified with the $f_0(975)$ meson for concreteness. The value of g is the measured pion-nucleon pseudoscalar coupling constant. With these values, the non-linear self-interaction strength has a large value, $\lambda \approx 91$.

For a large-N_c treatment, the Gell-Mann-Levy model needs to be modified in the following two ways. First, as discussed in Sec. III, the pseudoscalar πN coupling is inappropriate, and should be replaced by pseudovector coupling as in Eq. (21), with $g_\pi = g/(2M_N) = 1.42$ fm. Unfortunately, with this replacement chiral symmetry is lost, even for $\alpha = 0$. However, as stated in the introduction, our purpose in this paper is to explore the large-N_c approach in a multi-channel model, not to present a fully realistic effective Lagrangian of the low-lying hadrons, which would require not only approximate chiral symmetry but also the incorporation of vector mesons. (To look at the bright side, the fact that we are sacrificing chiral symmetry re-emphasizes the point that our large-N_c techniques have nothing to do with the chiral limit.)

Second, the meson couplings to the nucleon must be augmented by suitable couplings to the entire $I = J$ baryon tower (and likewise for the nucleon kinetic energy). The prescription for doing so is Eq. (23) for the pion. It is easy to check that the analogous prescription for the σ is given simply by

$$-g\sigma\overline{N}N \;\longrightarrow\; -g\sigma\int_{SU(2)} dA\;|A\rangle\,\langle A|\;. \tag{39}$$

As previously, we solve for the classical meson fields, for the reference choice of collective coordinate $A = 1$, by means of a hedgehog ansatz:

$$\pi^a_{\rm cl}(\mathbf{x}) = \hat{\mathbf{r}}^a F(r)\;, \quad \sigma_{\rm cl}(\mathbf{x}) = G(r)\;. \tag{40}$$

Smearing out the δ-function baryon source as in Eq. (19), we find coupled non-linear Euler-Lagrange ODE's for F and G:

$$\frac{d^2}{dr^2}F + \frac{2}{r}\frac{d}{dr}F - \left(\frac{2}{r^2} + m_\pi^2\right)F - \lambda\left[F^3 + FG^2 + 2vFG\right] = -\frac{3gr}{M_N a_N^5 \pi^{3/2}}\exp\left(-r^2/a_N^2\right) \tag{41a}$$

$$\frac{d^2}{dr^2}G + \frac{2}{r}\frac{d}{dr}G - m_\sigma^2\,G - \lambda\left[G^3 + F^2G + 3vG^2\right] = \frac{g}{(a_N\sqrt{\pi})^3}\exp\left(-r^2/a_N^2\right) + \lambda v F^2\;. \tag{41b}$$

We will generally set the nucleon size parameter $a_N = 0.52$ fm, but we will also consider the dependence of our results on a_N in Sec. VI(C) below. The boundary conditions are that F and G must be regular at the origin and exponentially decaying (rather than growing) at infinity. The classical pion profile $F(r)$ falls off like $\exp(-m_\pi r)/r$ at large distances. On the other hand, $G(r)$ falls off not like $\exp(-m_\sigma r)/r$ as one might naively expect, but rather like $\exp(-2m_\pi r)/r^2$ due to the F^2 source term on the right-hand side of Eq. (41b), and the fact that $2m_\pi < m_\sigma$. Details of our numerical "shoot and match" procedure for solving Eq. (41) can be found in Appendix A.

The solution for $F(r)$ and $G(r)$ is shown in Fig. 12. Note that $G(r)$ is negative with respect to $F(r)$ and v. It is this relative sign that leads to the attractive πN interaction found in this model.

V. PION-HEDGEHOG SCATTERING

Having solved for the classical pion and σ fields, we turn to the small-fluctuations problem of meson-baryon scattering. As in the Skyrme model [19–22], one first solves for meson-*hedgehog* scattering, and subsequently one folds in some group theory ($6j$ symbols) to obtain meson-*nucleon* scattering. The meson-hedgehog S-matrix is the topic of this Section, while the meson-nucleon S-matrix is the subject of Section VI to follow.

We return to the σ-π Lagrangian, Eq. (35) as modified subsequently in the text in the manner suggested by large-N_c. Consider fluctuations of the meson fields about their classical solutions,

$$\pi^a(x) \to \hat{\mathbf{r}}^a F(r) + \pi^a_{\rm qu}(x) \quad , \quad \sigma(x) \to G(r) + \sigma_{\rm qu}(x) \ . \tag{42}$$

Since F and G satisfy the Euler-Lagrange equations, terms linear in the fluctuating fields vanish. The quadratic terms then lead to linear equations of motion for $\pi^a_{\rm qu}(x)$ and $\sigma_{\rm qu}(x)$. Higher-order nonlinearities in the meson fields are subleading in $1/N_c$, as previously noted.

We will work out the partial-wave scattering amplitudes factoring out a uniform time-dependence $\exp(-i\omega t)$ from all the fluctuating fields. For the σ this involves the usual expansion in spherical harmonics,

$$\sigma_{\rm qu}(\omega, \mathbf{x}) = \sum_{K,K_z} \phi_{KK_z}(\omega, r)\, Y_{KK_z}(\hat{\mathbf{x}}) \tag{43}$$

For the pions the decomposition is slightly more complicated [19–22]. The conserved quantum numbers are not isospin and total angular momentum but the so-called "grand spin," $\vec{K} = \vec{I} + \vec{J}$. Since pions are spinless, $\vec{J}$ is just $\vec{L}$, the orbital angular momentum. Thus the appropriate partial wave analysis for pions involves an expansion in terms of *vector* spherical harmonics,

$$\vec{\pi}_{\rm qu}(\omega, \mathbf{x}) = \sum_{K,K_z,L} \psi_{KK_zL}(\omega, r)\, \vec{\mathcal{Y}}^{\,L}_{KK_z}(\hat{\mathbf{x}}) \ , \tag{44}$$

where L runs over values $K-1$, K, and $K+1$.

For each value of K, the equations for the four radial wavefunctions ϕ_K, $\psi_{K,K}$, and $\psi_{K,K\pm1}$ might be expected to form a 4×4 coupled system, [6] but parity uncouples $\psi_{K,K}$ from the other three. It obeys

$$\frac{d^2}{dr^2}\psi_{K,K} + \frac{2}{r}\frac{d}{dr}\psi_{K,K} + \left[q_\pi^2 - \frac{K(K+1)}{r^2} - V_\pi(r) \right] \psi_{K,K} = 0 \ , \tag{45}$$

where

$$q_\pi^2 = \omega^2 - m_\pi^2 \quad \text{and} \quad V_\pi(r) = \lambda[F^2(r) + G(r)(2v + G(r))] \ . \tag{46}$$

The remaining 3×3 coupled system of equations[7] is best expressed in matrix form. Assembling $\psi_{K,K\pm1}$ and ϕ_K into the column vector

$$\Psi_K(r) = \begin{pmatrix} \psi_{K,K-1}(r) \\ \psi_{K,K+1}(r) \\ \phi_K(r) \end{pmatrix} \ , \tag{47}$$

---

[6] From now on we drop the K_z label on ϕ and ψ since the ensuing equations are independent of K_z.

[7] For the special case $K = 0$ this is a 2×2 as $\psi_{0,-1}$ does not exist.

we find[8]

$$\frac{d^2}{dr^2}\Psi_K + \frac{2}{r}\frac{d}{dr}\Psi_K + [\mathsf{Q}_K - \mathsf{V}_K]\cdot\Psi_K = 0 \ . \tag{48}$$

Here Q_K is the diagonal matrix

$$\mathsf{Q}_K = \mathrm{diag}\left(q_\pi^2 - \frac{(K-1)K}{r^2},\ \ q_\pi^2 - \frac{(K+1)(K+2)}{r^2},\ \ q_\sigma^2 - \frac{K(K+1)}{r^2}\right) , \tag{49}$$

and V_K is the symmetric potential energy matrix

$$\mathsf{V}_{11} = V_\pi(r) + 2\lambda F^2(r)\left(\frac{K}{2K+1}\right) \tag{50a}$$

$$\mathsf{V}_{12} = -2\lambda F^2(r)\left(\frac{\sqrt{K(K+1)}}{2K+1}\right) \tag{50b}$$

$$\mathsf{V}_{13} = 2\lambda F(r)(v+G(r))\left(\frac{K}{2K+1}\right)^{1/2} \tag{50c}$$

$$\mathsf{V}_{22} = V_\pi(r) + 2\lambda F^2(r)\left(\frac{K+1}{2K+1}\right) \tag{50d}$$

$$\mathsf{V}_{23} = -2\lambda F(r)(v+G(r))\left(\frac{K+1}{2K+1}\right)^{1/2} \tag{50e}$$

$$\mathsf{V}_{33} = V_\sigma(r) \ , \tag{50f}$$

where we have defined

$$q_\sigma^2 = \omega^2 - m_\sigma^2 \quad \text{and} \quad V_\sigma(r) = \lambda[F^2(r) + 3G(r)(2v+G(r))] \ . \tag{51}$$

Note that q_σ^2 can be positive or negative, depending on whether the energy ω is above or below the σ threshold.

The "diagonal" potentials V_π and V_σ are plotted in Fig. 13. They are repulsive at short distances and attractive at intermediate range. The factor of three in the definition of V_σ makes it about three times more repulsive and attractive than V_π. Note that the vertical scale is in inverse fermis; these are potential wells of depths about 6 and 2 GeV, respectively, which means there is substantial attraction in both the σN and πN systems. Also shown in Fig. 13 are the off-diagonal transition potentials V_{12} and V_{13} (but without K-dependent factors) which are comparable in size to the diagonal potentials.

Numerically, the uncoupled equation (45) is readily solved using the Runge-Kutta technique employed in Secs. II and III. This method also works for the coupled equations (48),

---

[8] In so doing we are greatly assisted by the vector spherical harmonic identities, Eq. (10), in Ref. [21]. Note a typo there: K in the numerator of the square-root in the middle line of Eq. (10) should instead be $K+1$.

but only *above* the σ-threshold, $\omega > m_\sigma$. The problem below threshold is to ensure that the σ wavefunction remains exponentially decaying,

$$\phi_K(r) \to \exp(-\kappa r)/r \ , \quad \kappa = (m_\sigma^2 - \omega^2)^{1/2} \ . \tag{52}$$

In our experience, numerical noise in the Runge-Kutta integration invariably induces exponential blow-up: $\phi_K(r) \to \exp(+\kappa r)/r$. We emphasize that even below threshold the σ cannot be neglected as it causes substantial attraction in the πN channel. (Recall that the "box diagram" for $\pi N \to \sigma N \to \pi N$, Fig. 2c, is attractive.)

A numerically more robust approach that works both above and below the σ-threshold is to convert Eq. (48) into a set of coupled Fredholm integral equations of the second kind,

$$\Psi_K^{(i)}(r) = \mathcal{J}_K^{(i)}(r) + \int \mathsf{G}_K(r,r')\mathsf{V}_K(r')\Psi_K^{(i)}(r')\,dr' \ , \tag{53}$$

where the index i labels the linearly independent choices of inhomogenous driving terms. Above the σ threshold, i runs over 1,2,3 and the inhomogeneous terms are

$$\mathcal{J}^{(1)}(r) = \begin{pmatrix} \hat{\jmath}_{K-1}(q_\pi r) \\ 0 \\ 0 \end{pmatrix} \ , \quad \mathcal{J}^{(2)}(r) = \begin{pmatrix} 0 \\ \hat{\jmath}_{K+1}(q_\pi r) \\ 0 \end{pmatrix} \ , \quad \mathcal{J}^{(3)}(r) = \begin{pmatrix} 0 \\ 0 \\ \hat{\jmath}_K(q_\sigma r) \end{pmatrix} \ . \tag{54}$$

Below threshold, only the first two of these should be kept. The multi-channel Green's function G_K is the diagonal matrix

$$\begin{aligned}
\mathsf{G}_{11}(r,r') &= -\frac{1}{q_\pi}\hat{\jmath}_{K-1}(q_\pi r_<)\hat{n}_{K-1}(q_\pi r_>) \ , \\
\mathsf{G}_{22}(r,r') &= -\frac{1}{q_\pi}\hat{\jmath}_{K+1}(q_\pi r_<)\hat{n}_{K+1}(q_\pi r_>) \ , \\
\mathsf{G}_{33}(r,r') &= -\frac{2}{\pi\kappa}\hat{\imath}_K(\kappa r_<)\hat{k}_K(\kappa r_>) \ , \text{ below threshold} \ , \\
\mathsf{G}_{33}(r,r') &= -\frac{1}{q_\sigma}\hat{\jmath}_K(q_\sigma r_<)\hat{n}_K(q_\sigma r_>) \ , \text{ above threshold} \ .
\end{aligned} \tag{55}$$

where $\hat{\jmath}_l$, $\hat{n}_l$ are spherical Ricatti-Bessel functions [38] and $\hat{\imath}_l$, $\hat{k}_l$ are modified spherical Ricatti-Bessel functions [39], regular at the origin and exponentially decaying, respectively. By design, the multi-channel Green's function assures regularity of the wave functions at the origin *and* the asymptotic exponential fall-off of the ϕ_K below the σ threshold. Note that G_{33} is continuous through the threshold.

The S-matrix for the uncoupled pion scattering, Eq. (45), will be denoted here as the single-subscript quantity S_K, where the orbital angular momentum quantum numbers $L =$

$L' = K$ are suppressed. It is derived from the asymptotic analysis of the wavefunction in the usual way. The corresponding phase-shift δ_K, defined as

$$S_K = e^{2i\delta_K} \ , \tag{56}$$

is plotted against pion momentum k in Fig. 14 for $K \leq 5$. For each K the corresponding phase shift is attractive, if numerically small apart from the case $K = 1$, and comparatively much less significant than in the Skyrme model (*cf.* Fig. 1, Ref. [21]). As always in scattering problems, the centrifugal barrier term in the scattering equations delays the onset of the rise in the phase-shift for the higher-L partial waves.

The coupled-channels 3×3 (above threshold) or 2×2 (below threshold) part of the S-matrix will be denoted S^K_{ij}, $i, j = 1, 2$ and/or 3, according to $L = K - 1, K + 1$, and/or K. It is obtained as follows. First, the K^K-matrix is formed according to

$$\mathsf{K}^K_{ij} = -(1/q_j) \int dr \, \hat{\jmath}_L(q_j r)[\mathsf{V}(r)\Psi^{(i)}(r)]_j \ , \tag{57}$$

where $L = K - 1, K + 1$ and/or K for $j = 1, 2$ and/or 3, respectively, and also $q_1 = q_2 = q_\pi$, $q_3 = q_\sigma$. From the K^K-matrix, the S-matrix is formed in the usual way,

$$\mathsf{S}^K_{ij} = (q_j/q_i)^{1/2}[(1 - i\mathsf{K}^K)(1 + i\mathsf{K}^K)^{-1}]_{ij} \ , \tag{58}$$

where for an explanation of the square-root flux factors (needed only for multichannel scattering) we refer the reader to Ref. [40]. Time-reversal invariance implies $\mathsf{S}^K = (\mathsf{S}^K)^T$, which we have found to be a stringent check on our numerics. We will parametrize S^K_{ij} as $\eta^K_{ij} \exp 2i\delta^K_{ij}$ subject to this symmetry property as well as to unitarity.

The phase-shifts corresponding to the specific S-matrix elements S^K_{11} and S^K_{22} are plotted in Figs. 15-16. Recall that, with our notation, these are the S-matrix elements that describe pion-baryon scattering (no 'in' or 'out' σ's, only intermediate σ's) in which the orbital angular momentum quantum number is preserved ($L = L'$), as opposed to changing up or down by two units (as it can for $\pi N \to \pi\Delta$). The bulk of the attraction in the present model, due primarily to the intermediate σ-meson states, shows up in the phase-shifts of Fig. 16, with $L = L' = K + 1$. Here one sees resonances (phase shifts rising rapidly through 90 degrees) in each partial wave. In the $L = L' = K - 1$ partial waves (Fig. 15), one also sees attraction, although not so strong as to produce resonances. The surprise here is in the channel $K = 1$, $L = L' = 0$, which reveals the presence of a *bound state* (Levinson's theorem). Once one folds in the appropriate group theory in the following Section to project the hedgehog onto physical baryons, the existence of such a bound state manifests itself as a parity conjugate to the nucleon. This feature is, unfortunately, *not* found in Nature, nor in the Skyrme model, and is an unwanted, unphysical artifact of the present strongly-coupled σ-π model.

On the other hand, an *improvement* over the Skyrme model is the fact that all these phase-shifts (as well as those not plotted) eventually return to zero for sufficiently high energies. In contrast, in the Skyrme model they apparently grow without bound, eventually violating the unitarity constraints of quantum field theory, although admittedly at energies where several key approximations made in Refs. [19–22], such as the neglect of skyrmion recoil, are clearly unwarranted.

Another point to note about Fig. 15 are the cusp effects due to the opening of the σ threshold at $\omega = 5$ fm^{-1}. This is most apparent in the $K = 1, L = 0$ phase shift, but the effect is present in the higher partial waves as well.

VI. πN ELASTIC SCATTERING

A. Group-theoretics for meson-nucleon scattering

In the previous Section we derived an S-matrix for the scattering of pions and σ's off hedgehogs. The scattering information is encoded in partial-wave amplitudes we called S_K and S^K_{ij} where S^K is a 2×2 matrix below the σ threshold and a 3×3 matrix above it (except when $K = 0$ in which case S^K is 1×1 or 2×2, respectively). The integer index K labels the vectorial sum of the incoming or outgoing meson's isospin and angular momentum. K is conserved when the meson scatters off an object with hedgehog symmetry, in the same way that orbital angular momentum L is conserved in scattering from a spherically symmetric potential.

Of course, what we are really interested is scattering, not from a hedgehog, but rather from a nucleon or Δ. The relationship between the two problems, "physical scattering" versus "hedgehog scattering," is contained in the following group-theoretic expression [19–24]:

$$S_{LL'\,RR'\,I_{\rm tot}J_{\rm tot}}(\omega) \;=\; \sum_K S_{KLL'}(\omega)\cdot(-)^{R'-R}[(2R+1)(2R'+1)]^{1/2}(2K+1) \times \left\{ \begin{array}{ccc} K & I_{\rm tot} & J_{\rm tot} \\ R & L & I \end{array} \right\} \left\{ \begin{array}{ccc} K & I_{\rm tot} & J_{\rm tot} \\ R' & L' & I' \end{array} \right\} . \qquad (59)$$

Here ω is the meson energy in the baryon rest frame (baryon recoil being subleading in $1/N_c$), L (L') is the initial (final) orbital angular momentum, I (I') is the isospin of the incoming (outgoing) meson, and R (R') is the spin/isospin of the initial (final) $I = J$ baryon (e.g., $R = 1/2$ for a nucleon, $R = 3/2$ for a Δ, etc.). For physical scattering, K is no longer conserved; it is just a dummy of summation, constrained by the triangle inequalities

implicit in the $6j$ symbols.[9] Instead, the conserved quantities are, as they must be, the total meson+baryon isospin and angular momentum, $I_{\rm tot}$ and $J_{\rm tot}$. The S-matrix element on the left-hand side is a physical partial-wave amplitude that can be compared directly with experiment. The "reduced S-matrix" under the summation is a meson-hedgehog amplitude, in slightly different notation than that of the previous Section. The relation between the two notations is: when the incoming and outgoing mesons are each pions, then $S_{KKK} = S_K$, $S_{K,K-1,K-1} = \mathsf{S}^K_{11}$, $S_{K,K+1,K+1} = \mathsf{S}^K_{22}$, $S_{K,K-1,K+1} = S_{K,K+1,K-1} = \mathsf{S}^K_{12}$; when they are both σ's then $S_{KKK} = \mathsf{S}^K_{33}$; and when the incoming meson is a pion and the outgoing meson is a σ, then $S_{K,K-1,K} = \mathsf{S}^K_{13}$ and $S_{K,K+1,K} = \mathsf{S}^K_{23}$; with all other elements vanishing.

B. The Big-Small-Small-Big pattern

For the remainder of this paper we specialize to the elastic case $\pi N \to \pi N$. For each value of $L = L'$, there are then four *a priori* independent partial wave amplitudes, traditionally denoted $L_{2I_{\rm tot},2J_{\rm tot}}$. For example, in the case of F-wave scattering ($L = 3$) the four physical amplitudes are F_{15}, F_{17}, F_{35}, and F_{37}. But to leading-order in large-N_c, only two out of these four are independent. One can, for instance, solve for the two isospin-3/2 amplitudes as energy-independent linear combinations of the two isospin-1/2 amplitudes [19,22]; this is an example of the $I_t = J_t$ rule [26,27]. This holds in the Skyrme model, and because the group-theoretic expression (59) is the same, necessarily in the present σ-π model as well. These relations are reasonably well obeyed by the experimental πN partial-wave data [22], and are model-independent tests of large N_c.

Another interesting fact about the experimental data (see Fig. 4 *ff.*, Ref. [22]): If for each L one juxtaposes the four amplitudes in the above order, namely $L_{1,2L-1}$, $L_{1,2L+1}$, $L_{3,2L-1}$ and $L_{3,2L+1}$, then they reveal a striking pattern termed the "Big-Small-Small-Big" pattern. Namely, the outer two amplitudes, $L_{1,2L-1}$ and $L_{3,2L+1}$, are characterized by relatively large excursions of the S-matrix element through the Argand circle, while the inner two amplitudes, $L_{1,2L+1}$ and $L_{3,2L-1}$, show relatively much less motion. The Big-Small-Small-Big pattern is the single most consistent pattern characterizing the partial-wave S-matrix as a whole (the only clear exception to it being the D_{35}).

Reproducing the Big-Small-Small-Big pattern is one of the noteworthy successes of the

---

[9] Note: if either the incoming or the outgoing meson is a σ, then the associated $6j$ symbol has a zero in it and collapses to a product of Kronecker δ's. Conversely, the generalization of this expression to mesons that carry both isospin and spin, such as ρ's, involves $9j$ symbols, and is given in Ref. [24].

Skyrme model [21]. It is equally well reproduced by the present σ-π model, as we illustrate in Fig. 17. In fact, the pattern emerges for the same dynamical reason [22]: the fact that, for $K > 1$, in both the Skyrme model and in the σ-π model, the phase-shifts associated with S_{11}^{L+1} are much smaller than those of S_{22}^{L-1} (cf. Figs. 15-16). We therefore view it as a model-independent success of the large-N_c approach, whether one chooses to use skyrmions or explicit baryon fields.

C. The baryon spectrum of the large-N_c σ-π model

From the partial-wave amplitudes it is easy to extract the baryon resonance spectrum of the large-N_c σ-π model. Rather than record when the phase-shifts cross 90 degrees (a crude criterion sensitive to background potentials), a more robust definition of a resonance, adopted by experimentalists, is to look for Lorentzian peaks in the "speed plots," i.e., the plots of $|dT_{LI_{\rm tot}J_{\rm tot}}/d\omega|$ versus ω. The speed plots for a few selected partial waves are depicted in Fig. 18. Some peaks are unambiguous, whereas others are admittedly "in the eye of the beholder," but the same can be said about the corresponding experimental data.

Figure 19 displays the full resonance spectrum obtained in this fashion, through the H-waves ($L = 5$), limited to what we subjectively consider to be "two-star" resonances or better. The step-like structure, in blocks of alternating parity, is much more pronounced than in the Skyrme model, and certainly than in Nature. It can be partially accounted for by noting that, for $L > 1$, the reduced amplitudes of Fig. 16 dominate those of Figs. 14-15, so that for any fixed value of L, the resonance location in the four physical partial-wave amplitudes can be approximated by the resonance location in the single underlying reduced amplitude S_{22}^{L-1}. But this does not explain why the steps arrange themselves by definite parity (as we have indicated by the black bars below the horizontal axis), a feature for which we have no good understanding.

In general, the resonances in the σ-π model occur at substantially lower energies than in the Skyrme model, and in Nature. We have not explored the parameter space of our model [see Eq. (38)] in an attempt to rectify this disparity (as we are confident could be done), not just because of the computationally-intensive character of these multi-stage calculations, but also due to the frankly "toy" intent of this model, which we have constructed for illustrative purposes. We are optimistic that a more realistic model, incorporating the vector mesons, and properly implementing chiral symmetry, would be in better agreement with the observed baryon spectrum, while posing no significant additional conceptual or numerical difficulties beyond those we have already confronted herein.

The one parameter that we *have* experimented with is the nucleon size parameter a_N,

defined in Eq. (19), which acts as an ultraviolet cutoff. A variation from our nominal value $a_N = 0.52\,\mathrm{fm}$ to $a_N = 0.60\,\mathrm{fm}$ shows no discernible effect on the resonance positions, and only slight changes in the Argand plots themselves, primarily in the P-waves, one of which is shown in Fig. 20.

D. Some familiar problems

We have seen that this large-N_c σ-π model (and, we presume, others like it with explicit baryon fields) shares some notable successes with the Skyrme model—the Big-Small-Small-Big pattern, the energy-independent relations between the $I_{\rm tot} = 1/2$ and $I_{\rm tot} = 3/2$ πN amplitudes, the overall richness of the baryon resonance spectrum, etc. Moreover, the high-energy behavior of the partial wave amplitudes is much better than in the Skyrme model (see Sec. V). Not surprisingly, the σ-π model also shares some of the Skyrme model's failings. Figure 21 illustrates a specific partial wave amplitude in the σ-π model, juxtaposed with the experimental data. Obviously the real-world amplitude is much more inelastic than the present model. This is because, in the higher partial waves especially, multiple pion production soon dominates the experimental πN amplitudes. Yet, *formally*, processes such as $\pi N \to \pi\pi\pi N$ are down by powers of $1/N_c$ compared with $\pi N \to \pi N$, and are therefore entirely absent from leading-order theoretical treatments such as the present paper—as well as from the leading-order skyrmion treatments [19–23], which share the same problem. Below the σ threshold, the only source of inelasticity in the present model is the $\pi\Delta$ channel, exactly as in the Skyrme model. A theoretical means of summing at least *some* of the $1/N_c$ corrections, namely those associated with multiple pion production, would immeasurably improve either approach.

Just as serious is the failure of the σ-π model to bear even passing resemblance to experiment in the S and P waves. As is well known, these waves have been the "Achilles heel" of the Skyrme model too. Interestingly, whereas the Skyrme model shows *too few* resonances in these waves, the σ-π model errs in the opposite direction: *too many* resonances, particularly in the P_{13} and P_{31} waves, and including spurious bound states in the S_{31} and S_{11} channels as already noted in Sec. V. The interested reader is referred to Ref. [22] for a lengthy discussion of the problems in these lower waves in the Skyrme model, which are related, in part, to the failure to incorporate the translational and (iso)rotational recoil of the hedgehog (formally $1/N_c$ corrections, but numerically important). We expect that commentary to apply as well to models with explicit baryon fields. For example, the Weinberg-Tomozawa expression for the πN scattering lengths [41], which are predicted by current algebra, and which dominate the experimental S-wave amplitudes near threshold, formally appear only

at next-leading order in $1/N_c$ [22]. This suggests that if one were to start from an improved effective hadron Lagrangian that respects chiral symmetry (we remind the reader that the present σ-π model does *not*), and if one were to calculate to next-leading order in $1/N_c$, the most glaring disagreement with experiment in the S-waves ought to be repaired. Fixing the P-waves will require, at the least, (*i*) the splitting of the Δ from the nucleon (again, a $1/N_c$ effect), and (*ii*) the incorporation of the Compton-type diagrams, particularly Figs. 1a and 1b, the ameliorating effect of which has already been examined in the Skyrme model [11,12].

ACKNOWLEDGMENTS

We acknowledge valuable input from many of our colleagues, most notably Peter Arnold, Charles Benesh, Nick Dorey, Jim Friar, Terry Goldman, Gerry Hale, Jim Hughes, Marek Karliner, Arthur Kerman, Wim Kloet, Jim McNeil, Charles Price, Rob Timmermanns, and John Tjon. We also thank Aneesh Manohar for commenting on the draft.

This work has been supported by the Division of High Energy and Nuclear Physics, Energy Research, Department of Energy. MPM has also benefitted from an SSC Fellowship during part of the time we have been working on this problem.

REFERENCES

* E-Mail addresses: mattis@skyrmion.lanl.gov, silbar@lanl.gov.

[1] G. 't Hooft, Nucl. Phys. B72, 461 (1974) and B75, 461 (1974).

[2] G. Veneziano, Nucl. Phys. B117, 519 (1976); G. Rossi and G. Veneziano, Nucl. Phys. B123, 507 (1977).

[3] E. Witten, Nucl. Phys. B160, 57 (1979).

[4] S. Coleman and E. Witten, Phys. Rev. Lett. 45, 100 (1980); E. Witten, Nucl. Phys. B156, 269 (1979); P. Di Vecchia, Phys. Lett. B85, 357 (1979); G. Veneziano, Nucl. Phys. B159, 213 (1979).

[5] C. Carone, H. Georgi and S. Osofsky, Phys.Lett. B322, 227 (1994).

[6] M. A. Luty and J. March-Russell, hep-ph@xxx.lanl.gov/9310369; M. A. Luty, hep-ph@xxx.lanl.gov/9405271.

[7] T. H. R. Skyrme, Proc. Roy. Soc. A260, 127 (1961); Nucl. Phys. 31, 556 (1962).

[8] G. Adkins, C. Nappi and E. Witten, Nucl. Phys. B228, 552 (1983).

[9] P. B. Arnold and M. P. Mattis, Phys. Rev. Lett. 65, 831 (1990).

[10] N. Dorey, J. Hughes and M. Mattis, hep-ph@xxx.lanl.gov/9404274.

[11] D. I. Dyakonov, V. Yu. Petrov, and P. B. Pobylitsa, Phys. Lett. B205, 372 (1988).

[12] A. Hayashi, S. Saito and M. Uehara, Phys. Lett. B246, 15 (1990); Phys. Rev. D 43, 1520 (1991); ibid., D46, 4856 (1992); Prog. Theor. Phys. Supp. 109, 45 (1992); H. Riggs and H. Schnitzer, Phys. Lett. B305, 252 (1993).

[13] J.-L. Gervais and B. Sakita, Phys. Rev. Lett. 52, 87 (1984), Phys. Rev. D 30, 1795 (1984).

[14] R. Dashen and A. Manohar, Phys. Lett. B315, 425 (1993).

[15] R. Dashen and A. Manohar, Phys. Lett. B315, 438 (1993).

[16] R. Dashen, E. Jenkins and A. Manohar, Phys. Rev. D49, 4713 (1994).

[17] E. Jenkins, Phys. Lett. B315, 441 (1993).

[18] L. Schulman, Phys. Rev. 176, 1558 (1968).

[19] A. Hayashi, G. Eckart, G. Holzwarth and H. Walliser, Phys. Lett. B147, 5 (1984).

[20] B. Schwesinger, H. Weigel, G. Holzwarth and A. Hayashi, Phys. Rep. 173, 173 (1989).

[21] M. P. Mattis and M. Karliner, Phys. Rev. D 31, 2833 (1985).

[22] M. P. Mattis and M. Peskin, Phys. Rev. D 32, 58 (1985).

[23] M. Karliner and M. Mattis, Phys. Rev. D 34, 1991 (1986) and Phys. Rev. Lett. 56, 428 (1986); M. Karliner, Phys. Rev. Lett. 57, 523 (1986).

[24] M. P. Mattis, Phys. Rev. Lett. 56, 1103 (1986).

[25] J. T. Donohue, Phys. Rev. D37, 631 (1988).

[26] M. Mattis and M. Mukerjee, Phys. Rev. Lett. 61, 1344 (1988); M. Mattis and E. Braaten, Phys. Rev. D 39, 2737 (1989).

[27] M. Mattis, Phys. Rev. D 39, 994 (1989); Phys. Rev. Lett. 63, 1455 (1989).

[28] T.-S. H. Lee and F. Tabakin, Nucl. Phys. A191, 332 (1972), Table 1.

[29] V. Barger and M. Ebel, Phys. Rev. 138, B1148 (1965).

[30] R. Machleidt, K. Holinde and Ch. Elster, Phys. Rept. 149, 1 (1987).

[31] M. Lacombe, B. Loiseau, J. M. Richard, R. Vinh Mau, J. Cote, P. Pires, and R. De-Tourreil, Phys. Rev. C 21, 861 (1980).

[32] M. Gell-Mann and M. Levy, Nuovo Cimento 16, 705 (1960).

[33] B. Lynn, in Les Houches 1982, Proceedings, New Trends in Atomic Physics, Vol. 2, eds. G. Grynberg and R. Stora, North Holland, Amsterdam 1983, pp. 965-993.

[34] S. Weinberg, Phys. Lett. 251B (1990), Nucl. Phys. B357 (1991); C. Ordonez and U. van Kolck, Phys. Lett. B291: 459 (1992); B. W. Lynn, Nucl. Phys. B402, 281 (1993); B. W. Lynn and J. L. Friar, in preparation.

[35] R. R. Silbar and M. P. Mattis, in From Fundamental Fields to Nuclear Phenomena, ed. by J. A. McNeil and C. E. Price (World Scientific, Singapore, 1991), pp. 33-43.

[36] W. Press, B. P. Flannery, S. A. Teukolsky, and W. T. Vetterling, Numerical Recipes: The Art of Scientific Computing (Cambridge Univ. Press, New York, 1986).

[37] C. Rebbe and R. Slansky, Rev. Mod. Phys. 42, 68 (1970).

[38] J. R. Taylor, Scattering theory: the quantum theory of non-relativistic collisions, N.Y., Wiley, 1972.

[39] Milton Abramowitz and Irene A. Stegun, eds., Handbook of mathematical functions with formulas, graphs, and mathematical tables, N.Y., Dover, 1972; p. 227.

[40] J. R. Taylor, ibid., problem 19.5, p. 390, and section 20-b, pp. 398-404.

[41] S. Weinberg, Phys. Rev. Lett. 17, 168 (1966).

[42] R. R. Silbar, Comp. in Phys. 7, 592 (1993).

APPENDIX A: NUMERICAL AND COMPUTATIONAL DETAILS

1. Solving the coupled non-linear equations

We describe here the method we use for solving the non-linear classical field equations, Eq. (41), for the full σ-π model. (Exactly the same technique is used for the σ-only and π-only warm-up problems discussed before that point.) These are coupled ordinary nonlinear differential equations. The nonlinearity implies that there is some sensitivity in finding solutions; indeed, for some ranges of parameters, one may not be able to find solutions at all.

We are looking for solutions of these equations which are regular at the origin and which fall off asymptotically at large distances. Examining the indicial behavior of Eq. (41) near $r = 0$, we find that

$$F(0) = 0 \ , \qquad F'(0) = A \ , \qquad G(0) = B \qquad G'(0) = 0 \ . \tag{A1}$$

The indicial values A and B, along with asymptotic scale parameters C and D defined below in Eqs. (A2) and (A3), are initially unknown. Their values will be fixed by the non-linearity when we solve the differential equations.

As $r \to \infty$, the pion profile function is required to have the usual Yukawa-like fall-off,

$$F(r) \to C \exp(-m_\pi r)/r \ . \tag{A2}$$

Things are more complicated for $G(r)$ as $r \to \infty$ because the asymptotic behavior of $G(r)$ is governed by the coupling term to two pions. That is, it will fall off like $\exp(-2m_\pi r)/r^2$ rather than the faster $\exp(-m_\sigma r)/r$. After some analysis (solving a linearized Eq. (41b) using a Green's function technique with the $F^2(r)$ term on the right-hand-side providing the inhomogeneity),

$$G(r) \to D\frac{e^{-m_\sigma r}}{r} \ - \ \frac{\lambda v C^2}{2m_\sigma} \ \frac{e^{-2m_\pi r}}{r} E_1[-(m_\sigma + 2m_\pi)r] \ , \tag{A3}$$

where E_1 is an exponential integral [39].

The solution of Eq. (41) constitutes a two-boundary-value problem. We solve the equations using a standard shoot and match technique [36]. Not knowing, at first, the values for the "scale parameters" $A \ldots D$, we make an initial guess for their values and proceed to refine them with an iterative procedure.

The procedure is as follows. Given $A \ldots D$, we integrate out from the origin using a Runge-Kutta technique to our matching radius, r_m, which we choose to be a_N. We then Runge-Kutta integrate backwards to r_m from r_a, a point where the asymptotic forms

shown above are expected to hold. We typically choose r_a to be 2 fm. The values at r_m of F and G, and their derivatives, from the two integrations are then compared. The mismatches, or discontinuities, give four conditions which can be used to choose corrections to the guessed values of $A \ldots D$ that would drive the discontinuities toward zero. (This is a generalization to four variables of the Newton-Rapheson method; it requires four more passes of Runge-Kutta integrations to compute the derivatives of the discontinuities with respect to the scale parameters.) Correcting the $A \ldots D$ as calculated, one can repeat this process, hopefully getting a better, less discontinuous $F(r)$ and $G(r)$. The procedure is iterated until it converges to a solution.

The above iterative procedure was programmed in Fortran and was originally run as a batch job on a VAX-VMS minicomputer from a terminal command line. For small values of λ (i.e., small non-linear contributions) the program would converge reasonably well. However, as the non-linearity was increased, corresponding to values of λ given by Eq. (37), the convergence became more delicate. Thus, we found it useful to make the code more interactive, so that the user could watch plots of F and G at every stage of the iteration and, if the process were going astray, stop it and start again with a new set of starting scale parameters. The computing was transferred to a NeXT workstation and a NeXTSTEP front end to the Fortran program was developed [42]. With this front end to aid the user, it was much easier finding a solution for $\lambda = 91$.

2. Runge-Kutta Approach to the Scattering Differential Equations

The quantum scattering phase shifts in, say, the σ-only model of Sec. II, is given by the asymptotic form of the radial wave function determined by Eq. (20). This linear differential equation (and the coupled-channels variants of Secs. III and V) are readily solved by Runge-Kutta integration [36], simply by integrating out from the origin. Starting values are taken from the regular solution for the partial wave of the angular momentum K under consideration, i.e., with behavior like $\hat{\jmath}_K(qr) \propto r^{K+1}$. (The scale can be chosen arbitrarily because the equation is linear.)

At a large enough distance, typically 10 fm or so, the solution is well-approximated by a linear combination of $\hat{\jmath}_K(qr)$ and $\hat{n}_K(qr)$. Fitting the coefficients of these functions, one can then form the S-matrix element and thence compute the phase shift. For the coupled-channels case, the S-matrix is found using the procedure given, for example, in Ref. [21] utilizing matrices formed from these fitted coefficients.

3. Comments on Solving the Integral Scattering Equations

Numerically, Eq. (53) is solved using the Nystrom method [36]. For our three-rowed column vector, this procedure involves the inversion of a large $3N \times 3N$ matrix, where N is the number of meshpoints. The time to do that inversion goes like N^3. We found that reasonable accuracy (1% or better) in the extracted S-matrix elements is obtained with $N = 150$ mesh points. These are typically distributed as follows: 120 mesh points, evenly spaced, from $r = 0$ to 3 fm and 30 points, evenly spaced, from 3 to 10 fm.

In debugging the coding we found it very useful to verify that the S-matrix is not only unitary but also symmetric (a consequence of time reversal invariance). Another useful check on the code was to see that the scattering wave functions and S are continuous through the σ threshold and agree with the prediction of the Runge-Kutta method above the threshold.

APPENDIX B: FIGURE CAPTIONS

1. Compton-type graphs contributing to meson-baryon scattering. Henceforth, directed lines stand for baryons, all other lines are mesons. The baryons B, B' and B'' stand for three members of the $I = J$ tower of baryons. Fig. 1(d) contains a purely mesonic loop and so is subleading in $1/N_c$; Figs. 1(a)-(c) do not, and so contribute at leading order [9].

2. Exchange-type graphs contributing to meson-baryon scattering. Fig. 2(f) contains a purely mesonic loop and so is subleading in $1/N_c$; Figs. 2(a)-(e) do not, and so contribute at leading order. In this paper we explicitly sum all such leading-order graphs in a model containing both π and σ mesons.

3. Examples of exchange-type graphs contributing to (a) the baryon-baryon interaction, (b) the baryon-antibaryon interaction, and (c) the baryon-baryon-baryon interaction. As none of these particular graphs contains a purely mesonic loop, they all contribute to leading order in $1/N_c$, and can be summed using the methods of Ref. [9].

4. An uncrossed n-meson exchange graph included in the summation of Fig. 2. The shaded blobs contains meson self-interactions that do not concern us.

5. A specific "crossing" or "tangling" of Fig. 4, for $n = 4$. There are $n!$ such tanglings.

6. The sum of all $n!$ tanglings including Figs. 4-5. In all three figures, the contents of the shaded blob are held constant. classical sources.

7. The tree-level one-point function $\sigma_{\rm cl}$, where the baryon has been replaced by an external source $j(\mathbf{x})$.

8. The fluctuating field $\sigma_{\rm qu}$ propagating through the nontrivial background generated by $\sigma_{\rm cl}$. Vertices can be read off from the quadraticized Lagrangian, Eq. (15).

9. The profile function $\sigma_{\rm cl}(r) = G(r)$ for the σ-only model of Sec. II.

10. Phase shifts for the σ-only model, as a function of σ momentum, for model parameters $m_\sigma = 600\,\mathrm{MeV}$, $g = 13.6$, and $a_N = 0.5\,\mathrm{fm}$.

11. Classical profile $F(r)$ in inverse fermis for the π-only model of Sec. III.

12. Classical profile functions $F(r)$ and $G(r)$ for the σ-π model, with parameters as in text.

13. Diagonal and off-diagonal potentials appearing in the small-fluctuations equations.

14. The phase shifts δ_K plotted against meson momentum k in the baryon rest frame (recall that baryon recoil is subleading in $1/N_c$).

15. The phase shifts δ_{11}^K plotted against meson momentum k in the baryon rest frame.

16. The phase shifts δ_{22}^K plotted against meson momentum k in the baryon rest frame.

17. Argand plots for the four F-wave elastic πN partial wave amplitudes, illustrating the "Big-Small-Small-Big" pattern (the F_{15} and F_{37} are big, the others small).

18. Examples of speed plots for selected πN amplitudes, from which resonance positions are extracted.

19. The baryon spectrum of the σ-π model. The vertical axis measures excitation energy in MeV above the nucleon/hedgehog mass. Not pictured are the two spurious bound states in the S_{11} and S_{31} channels.

20. Dependence of the P_{11} amplitude on the nucleon size parameter a_N, for 0.52 and 0.60 fm (solid and dashed lines, respectively).

21. Comparison of G_{17} amplitude between the σ-π model (solid line) and experiment (dotted line). The pion kinetic energy for each curve ranges from 0 to 1600 MeV.

This figure "fig1-1.png" is available in "png" format from:

http://arXiv.org/ps/hep-ph/9405366v1

This figure "fig1-2.png" is available in "png" format from:

http://arXiv.org/ps/hep-ph/9405366v1

This figure "fig1-3.png" is available in "png" format from:

http://arXiv.org/ps/hep-ph/9405366v1

This figure "fig1-4.png" is available in "png" format from:

http://arXiv.org/ps/hep-ph/9405366v1

This figure "fig1-5.png" is available in "png" format from:

http://arXiv.org/ps/hep-ph/9405366v1

This figure "fig1-6.png" is available in "png" format from:

http://arXiv.org/ps/hep-ph/9405366v1

This figure "fig1-7.png" is available in "png" format from:

http://arXiv.org/ps/hep-ph/9405366v1

This figure "fig1-8.png" is available in "png" format from:

http://arXiv.org/ps/hep-ph/9405366v1

This figure "fig1-9.png" is available in "png" format from:

http://arXiv.org/ps/hep-ph/9405366v1

This figure "fig1-10.png" is available in "png" format from:

http://arXiv.org/ps/hep-ph/9405366v1

FIGURES

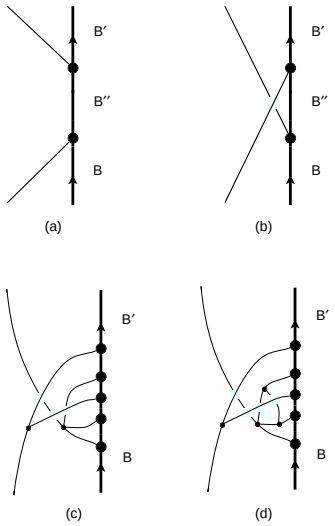

FIG. 1. Compton-type graphs contributing to meson-baryon scattering. Henceforth, directed lines stand for baryons, all other lines are mesons. The baryons B, B' and B'' stand for three members of the $I = J$ tower of baryons. Fig. 1(d) contains a purely mesonic loop and so is subleading in $1/N_c$; Figs. 1(a)-(c) do not, and so contribute at leading order [9].

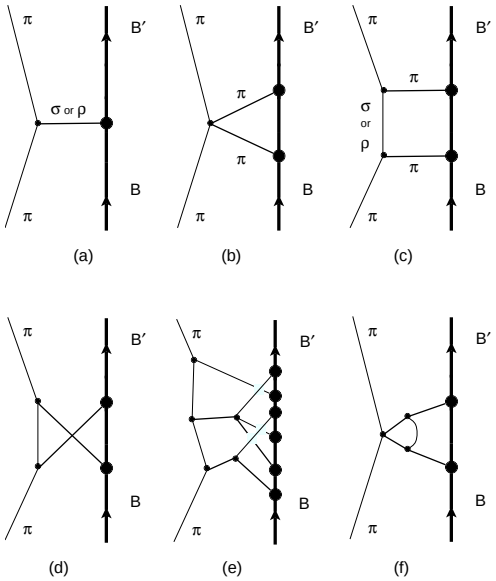

FIG. 2. Exchange-type graphs contributing to meson-baryon scattering. Fig. 2(f) contains a purely mesonic loop and so is subleading in $1/N_c$; Figs. 2(a)-(e) do not, and so contribute at leading order. In this paper we explicitly sum all such leading-order graphs in a model containing both π and σ mesons.

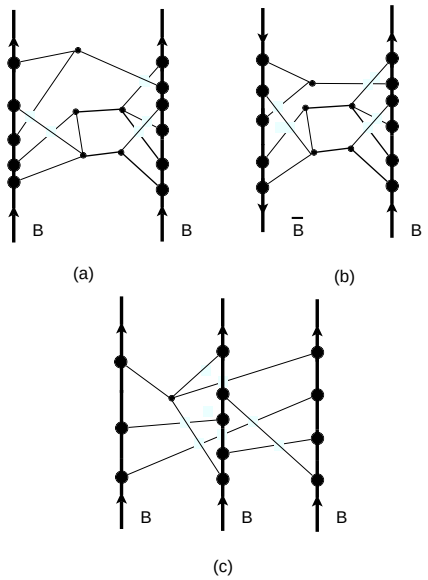

FIG. 3. Examples of exchange-type graphs contributing to (a) the baryon-baryon interaction, (b) the baryon-antibaryon interaction, and (c) the baryon-baryon-baryon interaction. As none of these particular graphs contains a purely mesonic loop, they all contribute to leading order in $1/N_c$, and can be summed using the methods of Ref. [9].

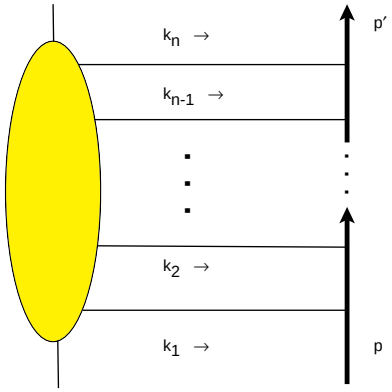

FIG. 4. An uncrossed n-meson exchange graph included in the summation of Fig. 2. The shaded blobs contains meson self-interactions that do not concern us.

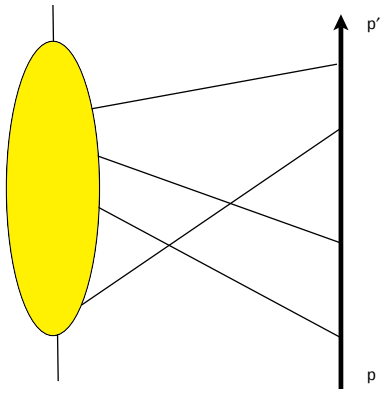

FIG. 5. A specific "crossing" or "tangling" of Fig. 4, for $n = 4$. There are $n!$ such tanglings.

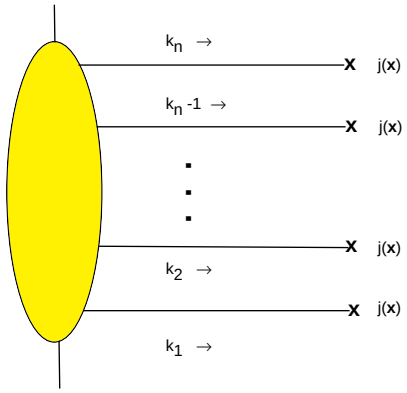

FIG. 6. The sum of all $n!$ tanglings including Figs. 4-5. In all three figures, the contents of the shaded blob are held constant. classical sources.

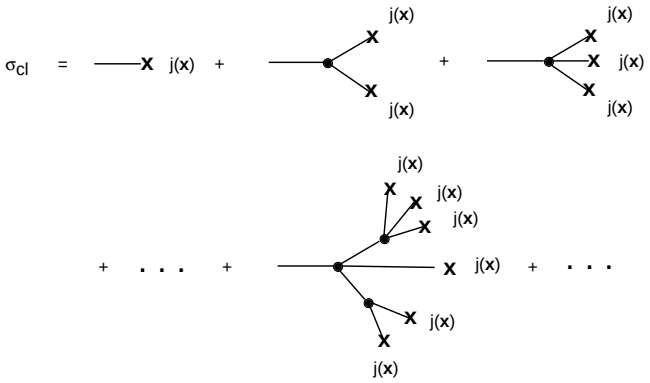

FIG. 7. The tree-level one-point function $\sigma_{\rm cl}$, where the baryon has been replaced by an external source $j(\mathbf{x})$.

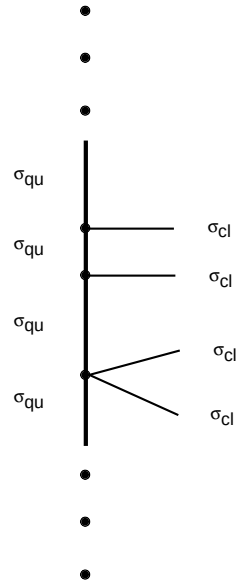

FIG. 8. The fluctuating field $\sigma_{\rm qu}$ propagating through the nontrivial background generated by $\sigma_{\rm cl}$. Vertices can be read off from the quadraticized Lagrangian, Eq. (15).

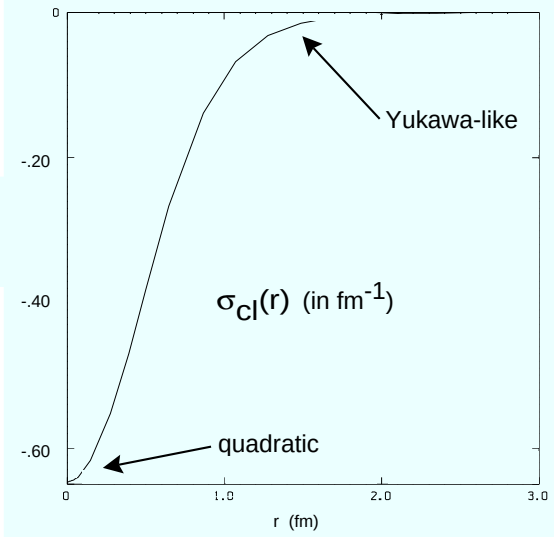

FIG. 9. The profile function $\sigma_{\rm cl}(r) = G(r)$ for the σ-only model of Sec. II.

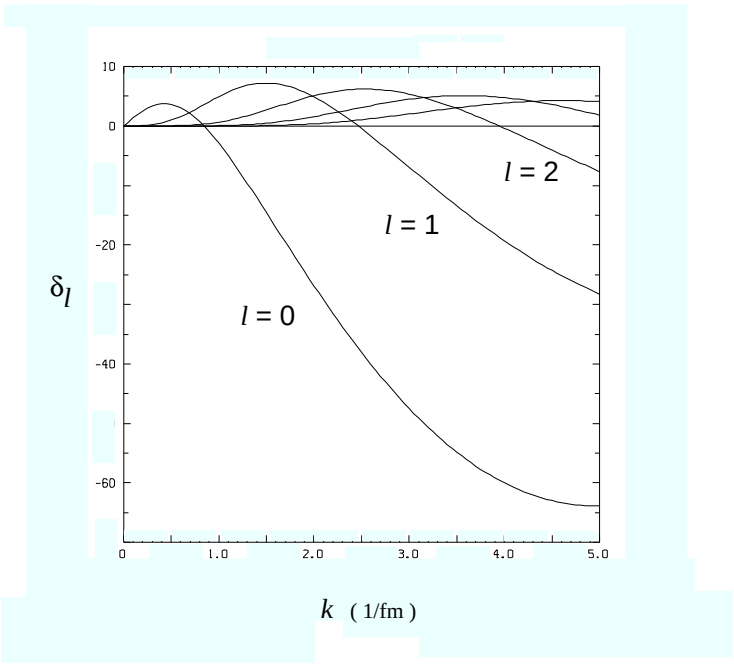

FIG. 10. Phase shifts for the σ-only model, as a function of σ momentum, for model parameters $m_\sigma = 600\,\mathrm{MeV}$, $g = 13.6$, and $a_N = 0.5\,\mathrm{fm}$.

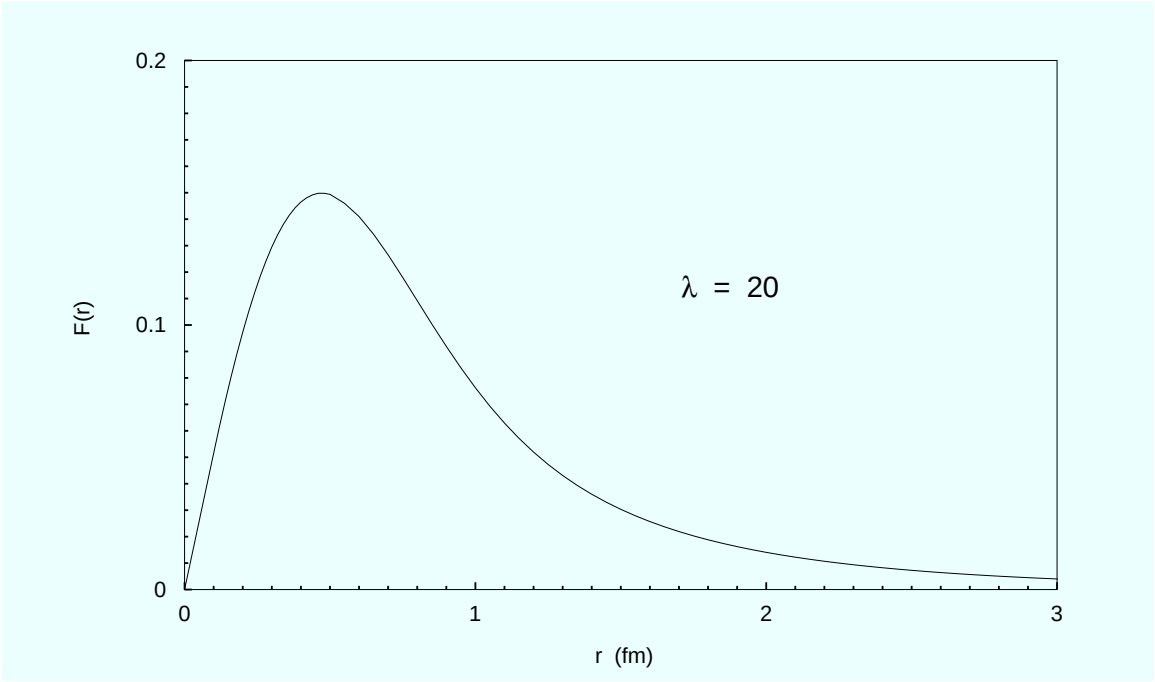

FIG. 11. Classical profile $F(r)$ in inverse fermis for the π-only model of Sec. III.

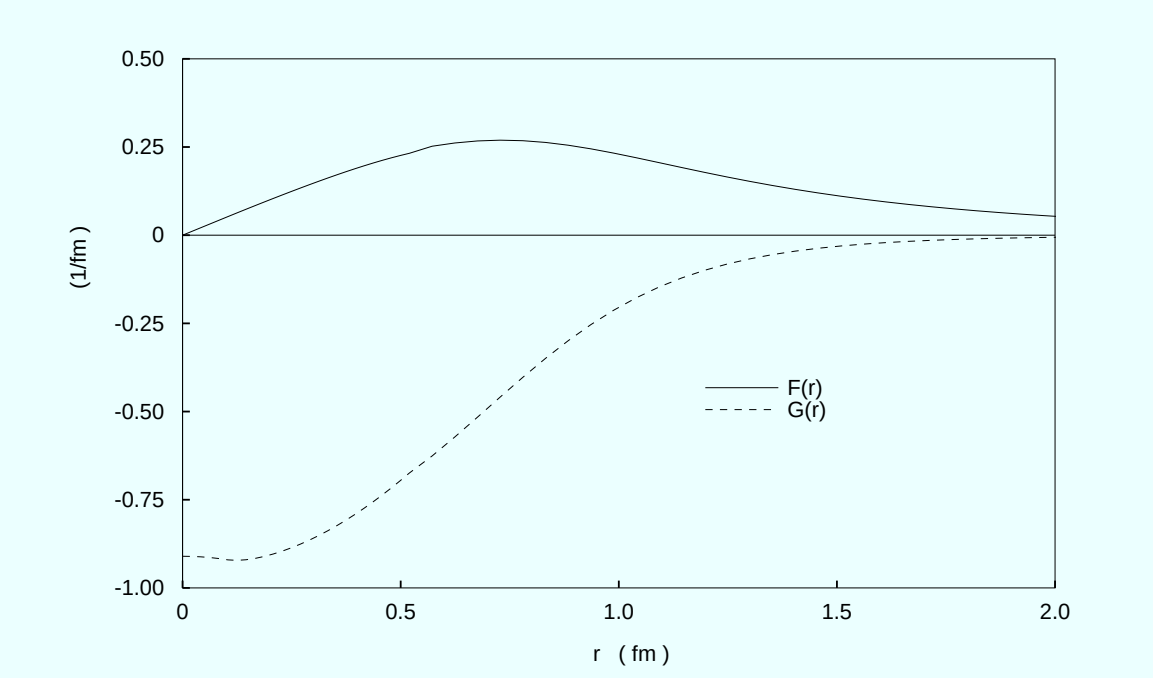

FIG. 12. Classical profile functions $F(r)$ and $G(r)$ for the σ-π model, with parameters as in text.

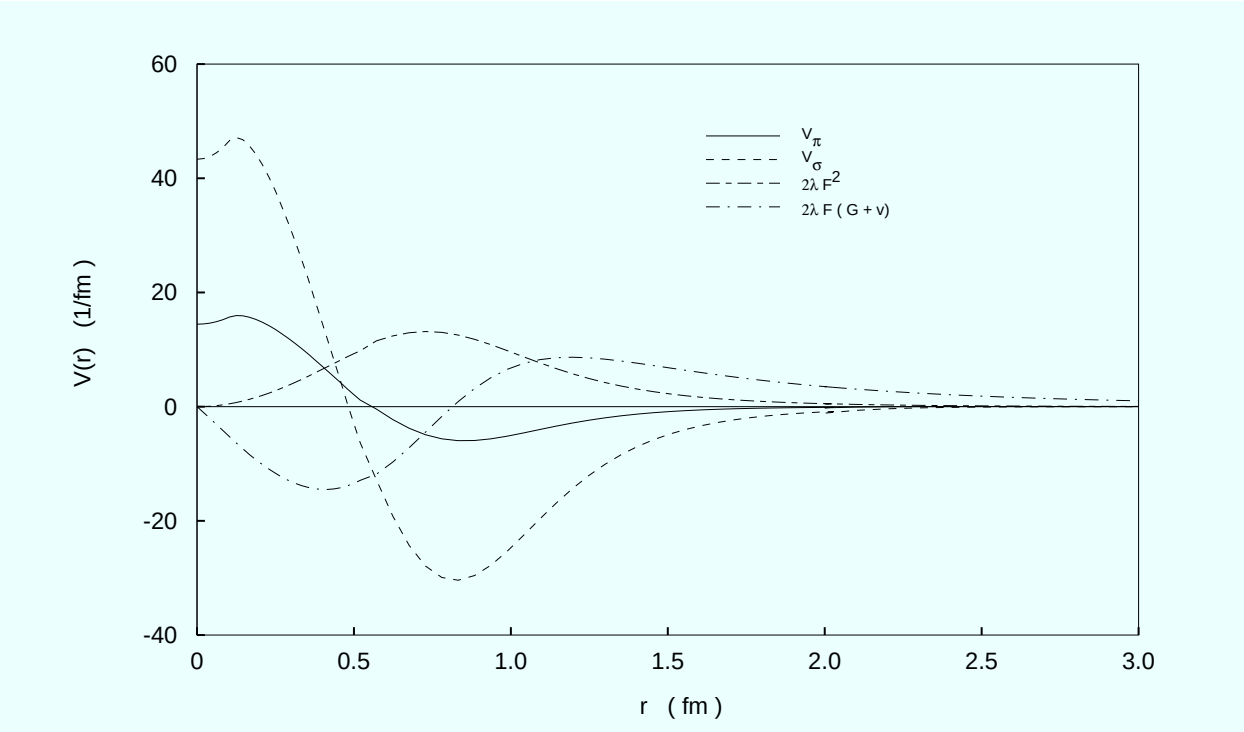

FIG. 13. Diagonal and off-diagonal potentials appearing in the small-fluctuations equations.

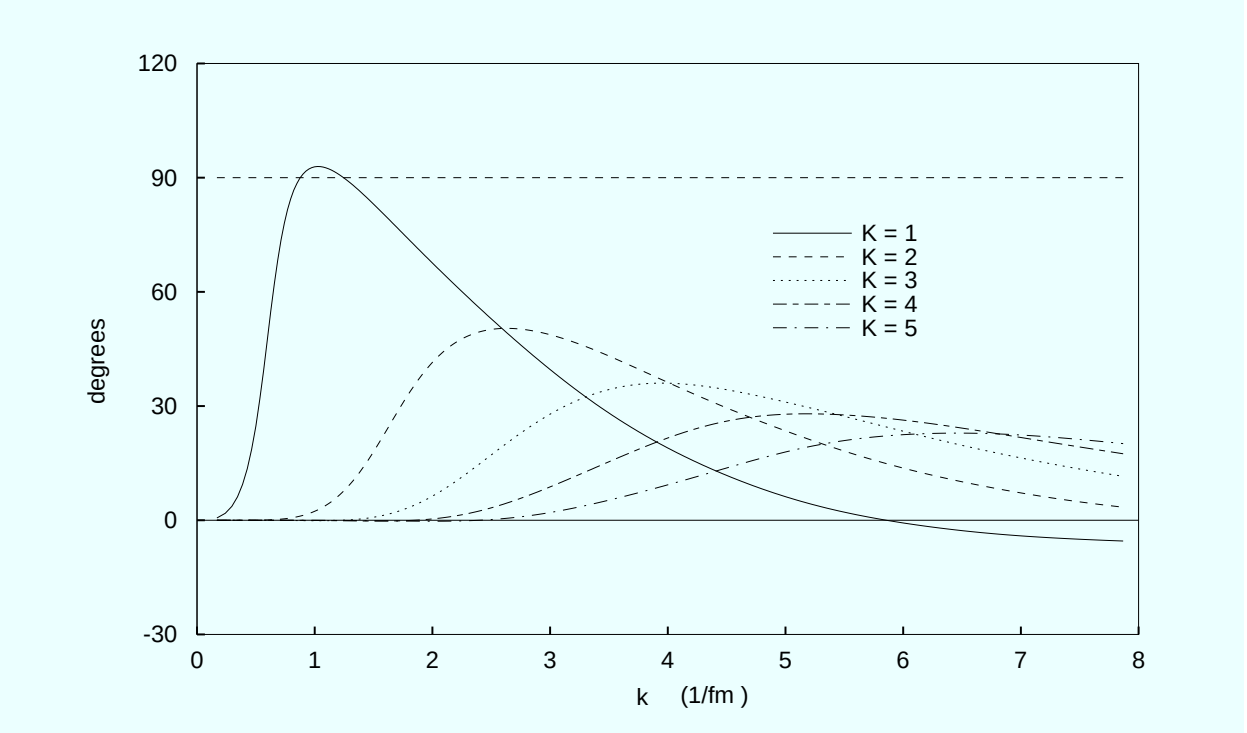

FIG. 14. The phase shifts δ_K plotted against meson momentum k in the baryon rest frame (recall that baryon recoil is subleading in $1/N_c$).

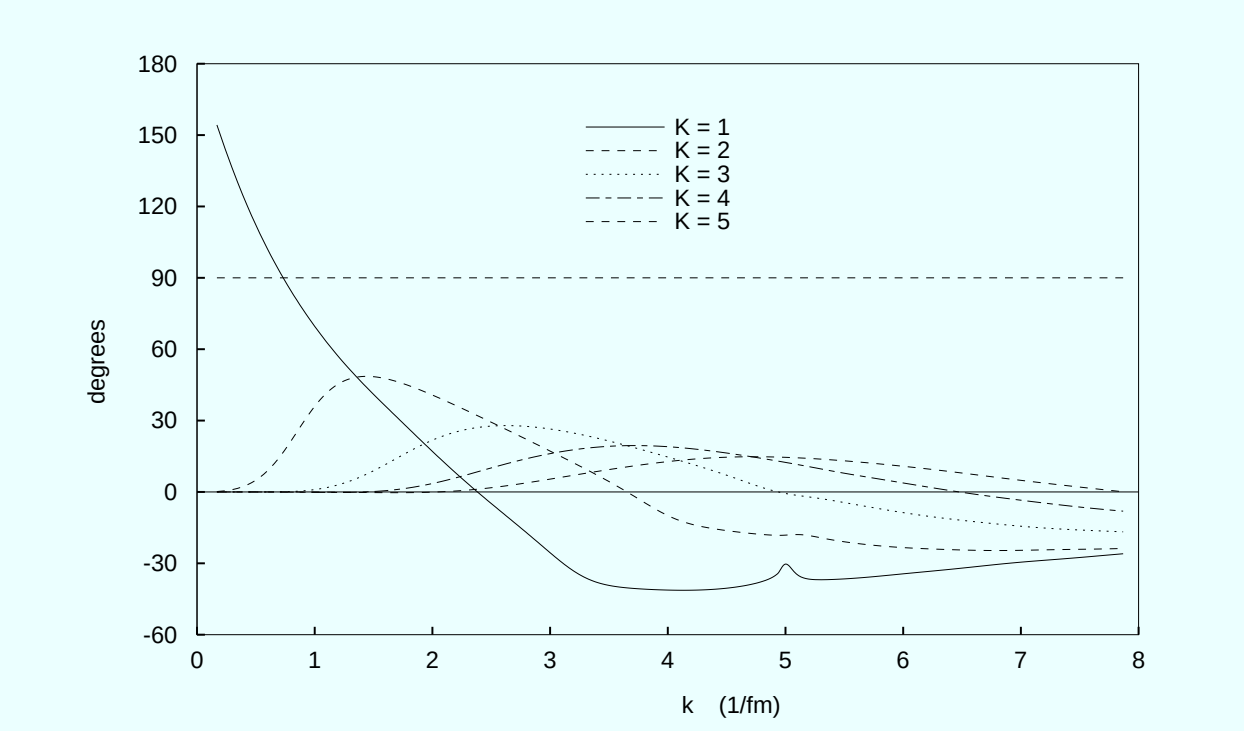

FIG. 15. The phase shifts δ_{11}^K plotted against meson momentum k in the baryon rest frame.

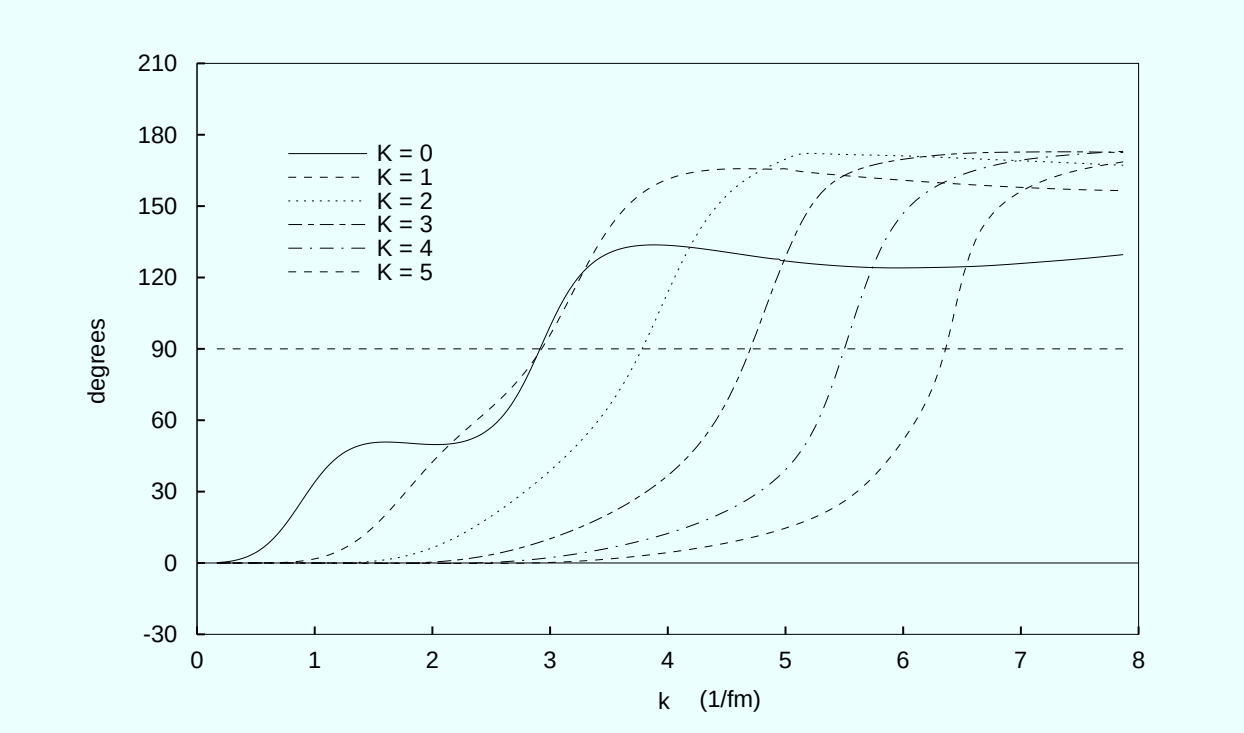

FIG. 16. The phase shifts δ_{22}^{K} plotted against meson momentum k in the baryon rest frame.

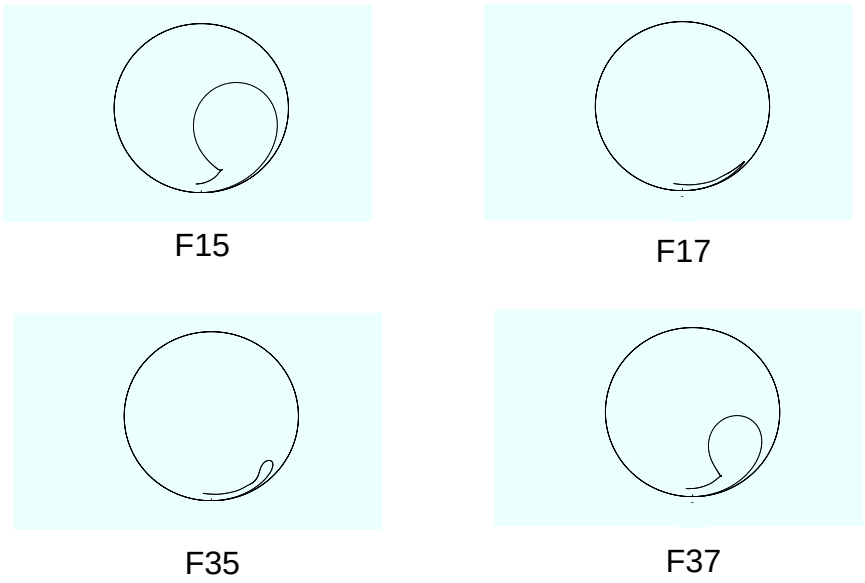

FIG. 17. Argand plots for the four F-wave elastic πN partial wave amplitudes, illustrating the "Big-Small-Small-Big" pattern (the F_{15} and F_{37} are big, the others small).

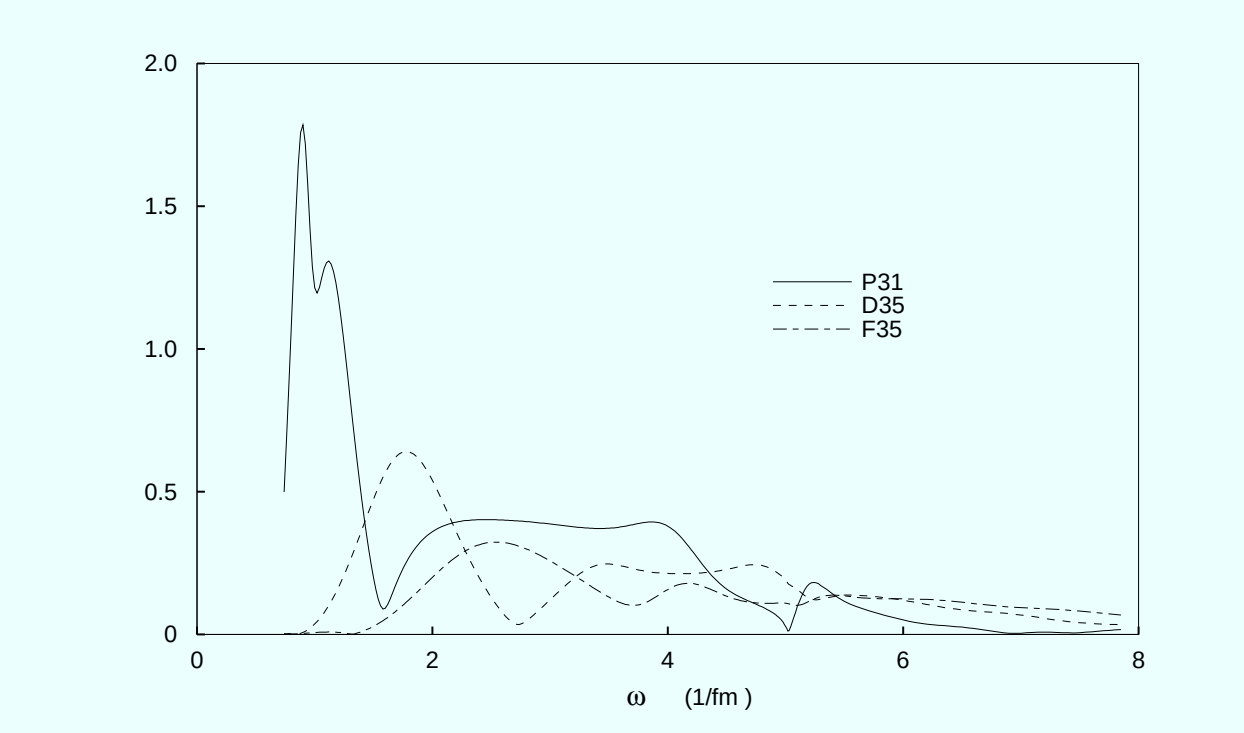

FIG. 18. Examples of speed plots for selected πN amplitudes, from which resonance positions are extracted.

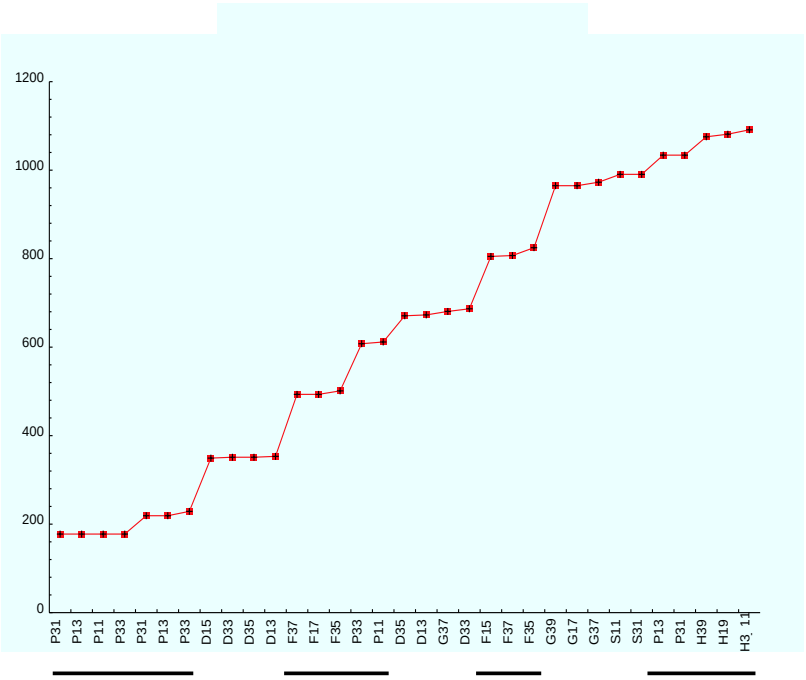

FIG. 19. The baryon spectrum of the σ-π model. The vertical axis measures excitation energy in MeV above the nucleon/hedgehog mass. Not pictured are the two spurious bound states in the S_{11} and S_{31} channels.

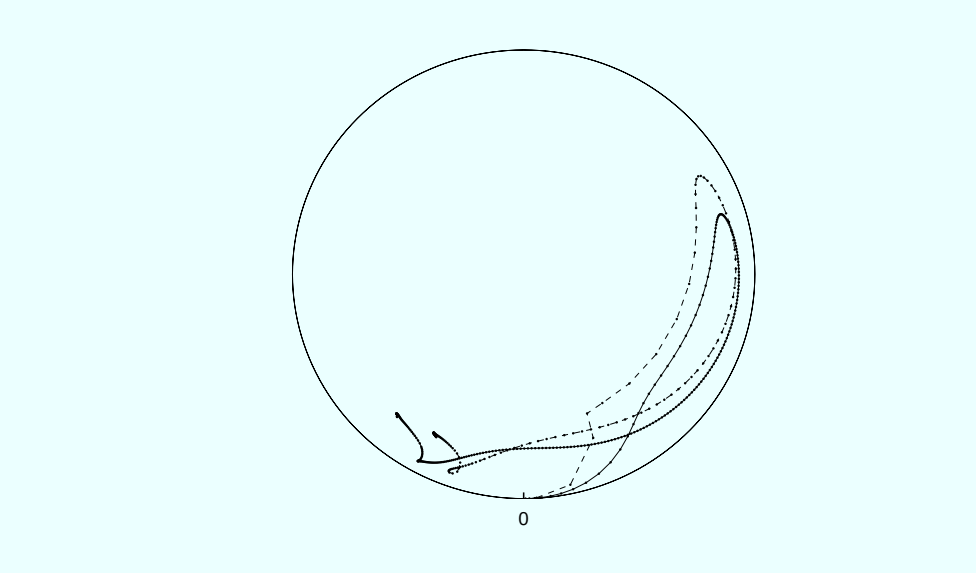

FIG. 20. Dependence of the P_{11} amplitude on the nucleon size parameter a_N, for 0.52 and 0.60 fm (solid and dashed lines, respectively).

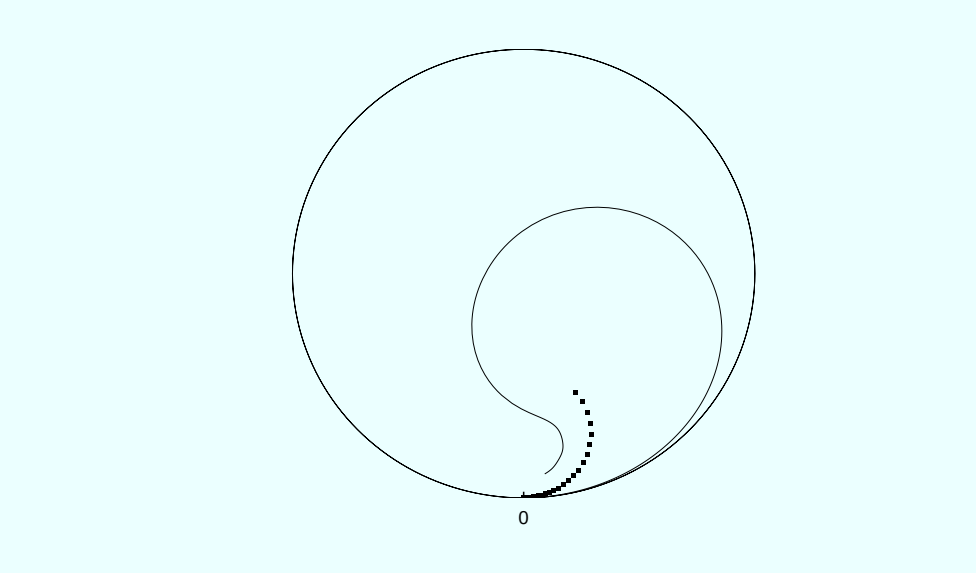

FIG. 21. Comparison of G_{17} amplitude between the σ-π model (solid line) and experiment (dotted line). The pion kinetic energy for each curve ranges from 0 to 1600 MeV.